FH University of Applied Sciences TECHNIKUM WIEN

# MASTER THESIS

Term paper submitted in partial fulfillment of the requirements for the degree of Master of Science in Engineering at the University of Applied Sciences Technikum Wien - Degree Program Tissue Engineering and Regenerative Medicine

# Application of a microfluidic CTC isolation technology to study neuroendocrine transdifferentiation in prostate cancer

By: Klara Bader, BSc
Student Number: 2010692013

Supervisor 1: FH-Prof. DI Dr. Carina Huber-Gries

Supervisor 2: David T. Miyamoto, MD, PhD

Vienna, Austria, December 8th, 2022

# Declaration of Authenticity

“As author and creator of this work to hand, I confirm with my signature knowledge of the relevant copyright regulations governed by higher education acts (see Urheberrechtsgesetz/ Austrian copyright law as amended as well as the Statute on Studies Act Provisions / Examination Regulations of the UAS Technikum Wien as amended).

I hereby declare that I completed the present work independently and that any ideas, whether written by others or by myself, have been fully sourced and referenced. I am aware of any consequences I may face on the part of the degree program director if there should be evidence of missing autonomy and independence or evidence of any intent to fraudulently achieve a pass mark for this work (see Statute on Studies Act Provisions / Examination Regulations of the UAS Technikum Wien as amended).

I further declare that up to this date I have not published the work to hand nor have I presented it to another examination board in the same or similar form. I affirm that the version submitted matches the version in the upload tool.”

Vienna, 08.12.2022

Place, Date


Signature

*"An experiment is a question which science poses to Nature,*
*and a measurement is the recording of Nature's answer."*

Max Planck

*"What I love about science is that as you learn, you don't really get answers.*
*You just get better questions."*

John Green

# Kurzfassung

Prostatakrebs ist weltweit die zweithäufigste Krebsart bei erwachsenen Männern. Ein tödlicher Subtyp des Prostatakrebses ist der neuroendokrine Phänotyp, der sich als Reaktion auf eine medikamentöse Hemmung der Androgenrezeptor-Signalübertragung aus einem Adenokarzinom entwickelt. Die molekularen Mechanismen, die der neuroendokrinen Transdifferenzierung zugrunde liegen, sind nach wie vor Gegenstand von Diskussionen. Es besteht ein hoher Bedarf an nicht-invasiver Methoden, um das Auftreten von behandlungsbedingter Abstammungsplastizität im Laufe der Zeit zu untersuchen. Liquid Biopsies bieten einen wiederholbaren, schmerzfreien Ansatz zur Probeentnahme von Tumorzellen. Zirkulierende Tumorzellen sind Krebszellen, die im peripheren Blut von metastatischen Prostatakrebs Patienten vorkommen. Diese Zellen können auf RNA-Ebene analysiert werden. Das Genexpressionsprofil von zirkulierenden Tumorzellen kann Aufschluss über mögliche Behandlungsreaktionen und -resistenzen geben. Die Suche nach zuverlässigen Biomarkern wird daher mehr Aufschluss über die neuroendokrine Transdifferenzierung geben und die klinische Behandlung der Krankheit weiter unterstützen.

In dieser Studie wurden zirkulierende Tumorzellen von 14 Patienten mit metastasierendem Prostatakrebs mit Hilfe des CTC-iChip mikrofluidisch erfasst. Die gewonnenen zirkulierenden Tumorzellen waren lebensfähig und intakt und wurden mittels ddPCR untersucht, um Genexpressionsprofile zu bestimmen. Mögliche neuroendokrine Hallmark-Gene wurden in der Literatur evaluiert und ddPCR-Assays für jedes dieser Gene entwickelt. Zusätzlich wurde gesundes Spenderblut aufbereitet und mit einzelnen Krebszellen versetzt, um das Verhalten von Prostatakrebspatientenproben zu imitieren. Hier konnte die Sensitivität der Assays nachgewiesen werden. Insgesamt wurde bei 42 % der Patienten eine Hochregulierung von neuroendokrinen Genen festgestellt.

Assays zum Nachweis von EZH2, MYC, PDX1, NEUROD1 und E2F1 erwiesen sich als ungeeignet für die Verwendung als Liquid Biopsy Marker. Die Daten weisen nach, dass digitale RNA-basierte PCR-Assays für DLL3, SYP und CHGA erfolgreich als Biomarker an Blutproben von Patienten mit metastasiertem Prostatakrebs eingesetzt werden können.

**Schlagwörter:** Prostatakrebs, Zirkulierende Tumorzelle, Mikrofluidik, CTC-iChip, Biomarker

# Abstract

Prostate Cancer is the second most prevalent cancer in adult men worldwide. A lethal subtype of prostate cancer is the neuroendocrine phenotype, which develops from adenocarcinoma in response to drug-induced androgen receptor signaling inhibition. The molecular mechanisms underlying neuroendocrine transdifferentiation still remain a subject of debate. There is an unmet need for non-invasive methods to study the emergence of treatment-induced lineage plasticity over time. Liquid biopsies offer a repeatable, painless approach to tumor sampling. Circulating tumor cells are cancer cells circulating in the peripheral blood of metastatic prostate cancer patients. These CTCs can be captured and analyzed on an RNA level. The gene expression profile of CTCs can give insights on possible treatment responses and resistance. Therefore, finding reliable biomarkers will give more insight on the neuroendocrine transdifferentiation and further help clinical disease management.

In this study, circulating tumor cells from 14 metastatic prostate cancer patients were microfluidically captured by using the CTC-iChip. The recovered CTCs were viable, intact, and were examined by ddPCR to determine gene expression profiles. Possible neuroendocrine hallmark genes were evaluated in the literature and ddPCR assays were designed for each of them. Additionally, we prepared healthy donor blood and spiked it with single cancer cells, to imitate the behavior of prostate cancer patient samples. Here we demonstrated the sensitivity of the assays. Overall, upregulation of neuroendocrine genes was found in 42% of patients.

Assays for detecting *EZH2, MYC, PDX1, NEUROD1,* and *E2F1,* were found to be unsuitable to use as liquid biopsy markers. The data suggest that digital RNA-based PCR assays for *DLL3*, *SYP*, *CHGA,* can be successfully applied as biomarkers to blood samples from metastatic prostate cancer patients.



**Keywords:** Prostate cancer, Circulating tumor cells, Microfluidics, CTC-iChip, Biomarker

# Acknowledgements

I want to thank my supervisor at Massachusetts General Hospital, David Miyamoto, MD, PhD, for having me as a student in his group. He has always been a wonderful mentor, who guided me through this exciting and interesting project and provided the mentorship to investigate the discovery of neuroendocrine biomarkers. I also want to give special thanks to Keisuke Otani, MD, PhD, whose advice, and support contributed greatly to this work. I want to thank the rest of the Miyamoto Lab for their encouragement and fun times at the lab. I want to thank all Labs of the Mass General Cancer Center for the interesting lab talks and the collaborative working environment.

My studies at the FH Technikum Wien were an inspiring time that gave me amazing education. I also want to give thanks to my other supervisor, Dr. Carina Huber-Gries, who provided helpful feedback, which I very much appreciate.
I want to thank everyone who made it possible for me to have this unforgettable experience of going abroad, especially to such a prestigious institutions as Harvard and Massachusetts General Hospital. This includes the Austrian Marshall Plan Foundation, which granted me a scholarship, and many others at the International Offices of MGH and the FH Technikum Wien.

Last but not least, I want to give special thanks to my family, friends, and particularly my girlfriend. I feel enormously grateful to have as many wonderful people in my life.

My time in Boston will always be a time I will look back fondly on. I will forever be thankful for this experience.

# Table of Contents

## Table of Contents

# 1 Introduction

## 1.1 General information on prostate cancer

### 1.1.1 History of prostate cancer and case statistics

Cancer is the second leading cause of death in the United States of America (USA) and is therefore considered a major public health issue. Since 1991, at its peak in the 20th century, the cancer death rate has decreased, for a total fall of 31%, because of improvements in early detection, novel treatments, and smoking reduction. This trend was interrupted in 2020, because of the repercussions of the COVID-19 pandemic. The partial closing of healthcare institutions has led to a delay in diagnosis and first-course treatment, which resulted in a temporary decrease in cancer incidence followed by a rise in advanced-stage cases and finally in heightened mortality. However, quantifying the effects of the pandemic will require data of the following several years to come [1].

In the 1990s a rapid rise in prostate cancer cases was reported (Figure 1A). These noticeable high rates can be traced back to the introduction of widespread prostate-specific antigen (PSA) testing in the group of previously unscreened men. The test has been approved as a diagnostic screening tool by the Food and Drug Administration (FDA) in the years before but has partially led to overdiagnosing patients. Elevated PSA levels in patients let physicians to suspect a malignancy, which in not all individuals was a correct diagnosis. A significant drop in PC incidence cases from 2007 to 2014 resulted from a reduction in PSA testing due to recommendations by the US Preventive Service Task Force. In 2017 their recommendation was updated and PSA-testing for men aged 55 to 69 years, or with a family history of PC was introduced [1], [2].

When assessing the prevalence of prostate cancer (PC) in 2020 (191.930 new cases in the USA) compared to 2021 (248.530 cases in the USA), a significant decline can be observed in numbers, which likely stems from the before mention reason of belated diagnosis (COVID-19 pandemic). In general, prostate cancer is the most common cancer in American men, accounting for 26% of new cancer cases. About 11% (in number 34.130 cases) of cancer-related deaths are related to the disease prostate cancer, which is the second deadliest cancer behind lung and bronchus cancer with 22% (69.410 cases) in 2021 in the USA [2].

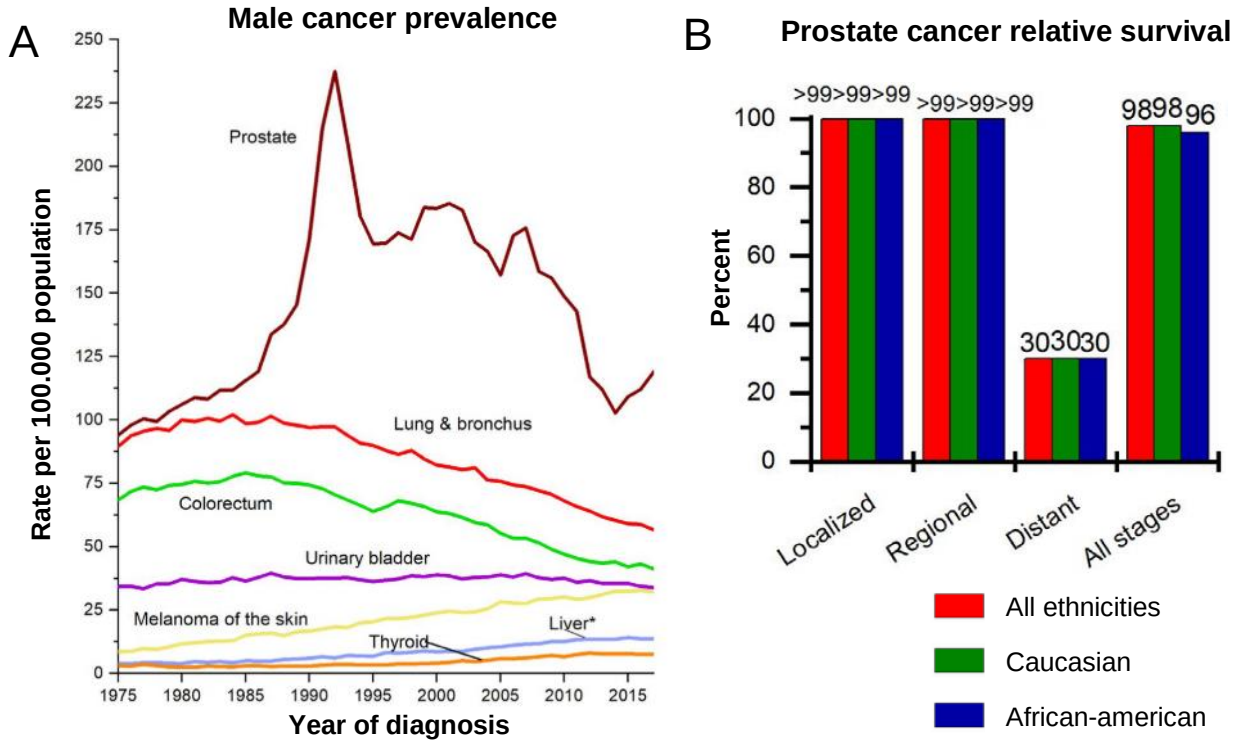


Figure 1: (A) Trends in cancer prevalence in the US from 1975 to 2017. The peak in prostate cancer incidence in the 1990s can be explained by the rise in prostate-specific antigen (PSA) testing, also diagnosing asymptomatic men. (B) The five-year survival rate of localized, regional, and distant prostate cancer stage displayed by race. Distant metastatic disease shows a drastic reduction in survival. Both graphical statistics taken from [1].

## 1.1.2 Cellular biology of the human prostate gland

To elaborate more on the prostate, an organ of the male reproductive system, some physiological information needs to be considered. The prostate gland is located underneath the bladder and surrounds the urethra (Figure 2A). One of its main functions is to produce essential secretions of semen, which retain sperm viability and formulate ejaculate. The prostate gland is composed of ducts and acini, which is a cluster of cells that mold a rounded end of an exocrine gland that produces secretion, embedded in the stroma. These acini and ducts consist of an individual columnar-shaped luminal epithelial layer, which is surrounded by a basal epithelial layer, which includes the basement membrane (Figure 2B) [3]. In the single layer of columnar epithelium, basal cells, intermediate cells, and neuroendocrine cells are also present. Smooth muscle myocytes are anchored to the basal lamina, which also connects to the stroma. Various cell types are present in the stroma such as fibroblasts, neurons, and endothelial cells [3], [4].

The outermost zone of the prostate gland is described as the peripheral zone, where 80% of tumors arise from (Figure 2A) [3]. In a cancerous state, but also in a normal state, epithelial cells in the prostate carry a high level of androgen receptor (AR). Prostate Cancer growth is driven by hormone dependency, that bind to AR. This mechanism will be discussed in detail

later in this introduction. Another trait of epithelial cells of the prostate is the secretion of PSA, which is transcriptionally activated by AR. As mentioned before, elevated PSA levels hint at prostate cancer presence in a patient [5].

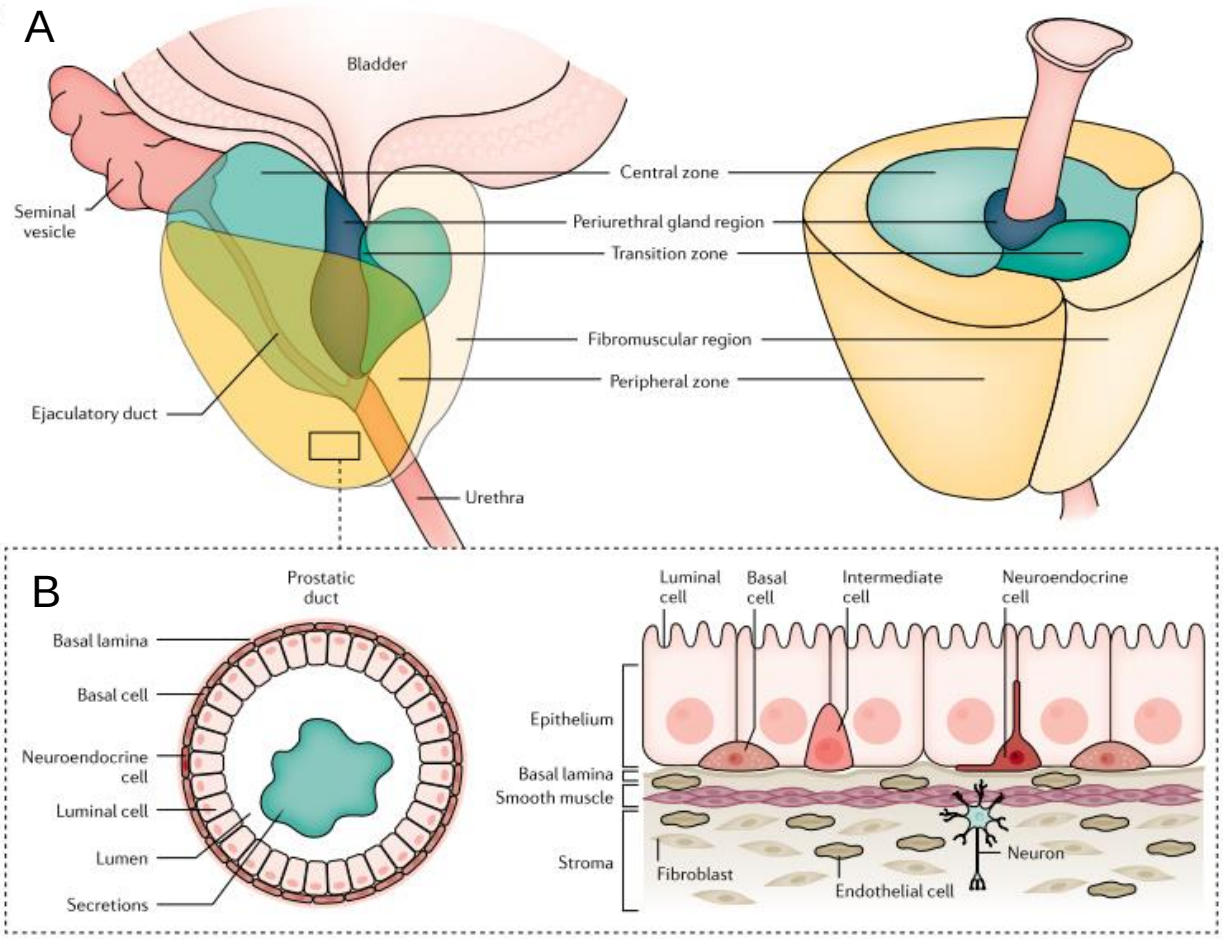


Figure 2: (A) Anatomy of the human prostate divided in five areas. Most cancerous tumors have their origin n the outlying peripheral zone. (B) The histological architecture of the prostate gland. Every duct and acini consists of several different cell types [3].

## 1.1.3 Prostate cancer diagnosis, stages, and survival

Other than measuring PSA levels, a digital rectal examination (DRE) is performed by a physician, and several other biomarker tests can be obtained from a blood draw analysis. Additionally, a magnetic resonance imaging scan (MRI) can be ordered to give patients clarity on their status. If previous abnormalities in the prostate are observed, a tissue biopsy from several regions of the prostate will be done to give a reliable diagnosis [3], [6].

To categorize prostate cancer stages, various parameters are used in the clinic. A very common pathological grading system is the Gleason score. Tumor architecture is graded by its histological differentiation status with a number between 1 and 5, 1 being well differentiated (healthy cell shape) and 5 being poorly differentiated (high-grad cancerous cell shape). The

grading of the two most prominent patterns is summarized as a low result (≤6), intermediate (7) or high (8-10) Gleason score. Another tool to describe a PC stage is the tumor-node-metastasis system (TNM). Essentially, this evaluation is based on tumor size and spreading reach [3], [6], [7].

The prognosis of survival for men suffering from prostate cancer varies strongly, depending on the tumor stage at primary diagnosis. About 80% of patients are being diagnosed with local organ-confined disease, 15% with locoregional disease and 5% with distant metastases. The factor of age has been identified as one of the biggest risk factors for being diagnosed with prostate cancer [1]. More than 85% of new cases are detected in individuals over the age of 60 years. Consequently, the disease prevalence is notably high in well-developed areas with a high life expectancy, like Europe, North America, Australia and certain regions in South America, such as Brazil. The worldwide incidence also correlates with the gross domestic product and following a Western diet. A very noticeable fact is, that racial ancestry is another big risk factor for being prone to prostate cancer. Men of Asian heritage, living in Asia have the least prostate cancer risk, whether Asian men living in the USA have a similar risk to white men. When looking at other demographics in the USA, men of Caribbean and African descent are at a twofold greater chance to be diagnosed early with a severely aggressive form of PC compared to white populations [1], [8].

The rate of mortality is high in developing nations, which may be caused by lack of screening, prevention and accessible care. To 5-year relative survival rate for localized and regional disease is over 99% in patients of various heritages (Figure 1B). Men who have been diagnosed with distant metastatic PC have a poor general survival rate of only 30% [1], [2].

## 1.2 Characteristic features of prostate cancer

### 1.2.1 Mutations in adenocarcinoma

Almost all prostate cancers develop from cells that line in the glandular tissue, this type of tumors are called adenocarcinomas. A particular cell of origin of human prostate cancer remains disputed. Some patients show morphological heterogeneity, whereby multiple tumor centers, that show genetic differences, can appear within one organ. Generally, metastases are believed to be clonally derived and, as a result mainly homogonous cellular populations. However, even metastases can carry genetically dissimilar subclones with divergent molecular features [9]. Tumor heterogeneity oftentimes occurs during or after standard care androgen deprivation therapy (ADT) and is a continued topic of research [10].

The critical factors of prostate cancer occurrence are believed to be somatic mutations in the basal, luminal or epithelial cell genome, which accumulate during a patient's lifetime. The named mutations primarily affect genes that regulate cell growth, cell proliferation, DNA damage response, and cell death. This state of abnormality in oncogenes and tumor suppressor genes results in defects in transcription and translation and further deregulated cell homeostasis [3], [11].

In localized prostate cancer patients, the most common domain for mutations is the AR-regulated promoter regions. In this area, a fusion of *TMPRSS2* and *ERG* is detected, in around 50% of localized patients. In tumorigenesis of metastatic disease, the two tumor suppressor genes *TP53* and *Rb1*, play a key role. In metastatic patients, *TP53* and *Rb1* are modified in 50% and 21% of the cases, respectively. Mutations in *TP53* and *Rb1* have shown strong evidence to drive disease progression and the formation of metastasis in lymph nodes [12].

### 1.2.2 Therapeutic approaches targeting androgen receptor

As previously mentioned, AR functions predominantly as a transcription factor, which is important for normal prostate function In malignant disease, prostate cancer is dependent on AR for tumor development, growth, and progression. This makes PC a uniquely targetable cancer by blocking the cascade of AR signaling [5]. Current treatments are able to do so in various ways, either blocking androgen synthesis or its actions throughout the body or reducing androgen production in the testicles [13]. Conventional androgen deprivation treatments include luteinizing hormone-releasing hormone (LHRH) agonists which bind LHRH receptor of the pituitary gland, which results in overstimulation before the gland stops LH production. Other drugs available are LHRH antagonists, which directly bind to the receptor, blocking the secretion of LH. ADT treatments are initially effective, until cellular resistance sets in due to AR mutations or amplifications. These mechanisms result in the suppression of serum testosterone to medical castration levels, and this state of disease is also called castration-resistant prostate cancer (CRPC) [3], [13].

In progressed metastatic disease the loss of AR signaling dependence leads to lineage plasticity of adenocarcinoma. The process of lineage plasticity (also transdifferentiation) describes the state where mature somatic cells de-differentiate and further re-differentiate into another cell lineage condition. In prostate cancer, this phenomenon is overserved when adenocarcinoma transforms into small-cell neuroendocrine (NE) phenotype (Figure 3). *De novo* NE prostate cancer is extremely rare, occurring in less than 1% of newly diagnosed patients. ADT-treatment-induced neuroendocrine prostate cancer (NEPC) is far more common with a prevalence of at least 10-17%, of CRPC patients evolving from adenocarcinoma [14], [15]. With a rising trend in occurrence, the clinical management of NEPC has gained attention from the research community.

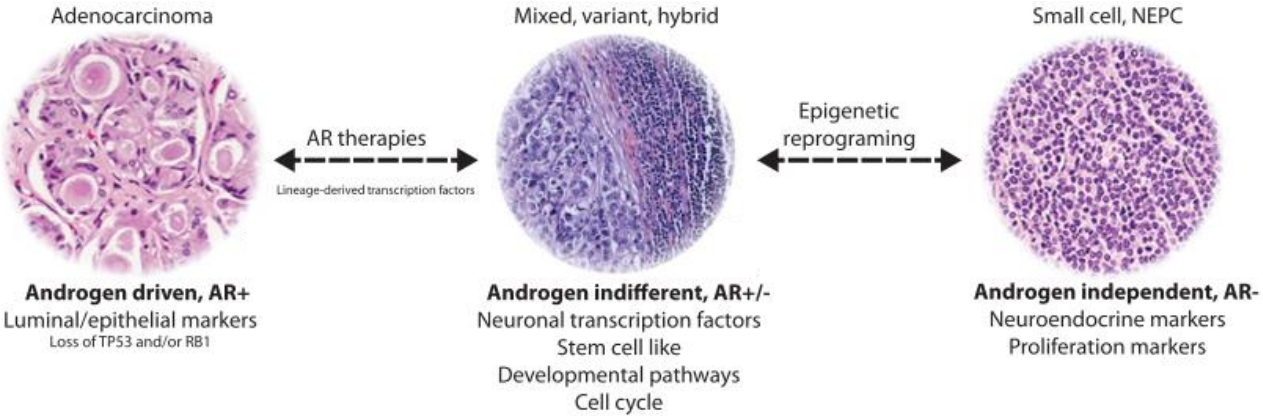


Figure 3: Progression of molecular signatures that arise in castration-resistant prostate cancer. Lineage plasticity is triggered by androgen deprivation therapy. During the transdifferentiation from adenocarcinoma to small-cell neuroendocrine prostate cancer (NEPC), the expression of androgen receptor (AR) is lost. Cellular hybrid forms of the tumor may arise during the process of transdifferentiation [16].

### 1.2.3 The cellular origin of neuroendocrine prostate cancer

In the past few decades, the origin of NEPC has been a highly discussed and controversial topic. Two central hypotheses are being investigated: the lineage plasticity hypothesis and the neuroendocrine cell hypothesis. The NE cell hypothesis proposes that NE cells, which make up a minor cell population of 1% in the epithelium of the prostate, are the ancestor of malignancy [17], [18]. NE cells and NEPC do share some similar features, for instance, the expression of NE markers, such as Synaptophysin (SYP) and Chromogranin-A (CHGA). This hypothesis was studied in a genetically engineered mouse model, where the animals developed metastasized NEPC in the lymph nodes. Even before disease initiation, and also after, the mice expressed SYP and CHGA markers. With this evidence given, this study identified epithelial NE cells in the prostate gland as the origin of malignant transformation [19]. In contrast to the neuroendocrine cell hypothesis stands the lineage plasticity hypothesis, which believes that the NE phenotype stems from spontaneous re-differentiation from adenocarcinoma [20], [21].

There has been significantly more research published supporting the theory of the lineage plasticity hypothesis [21].

Evidence has been generated by using genetically modified mouse models and patient-derived xenograft models, and additionally by investigating human prostate tissue studies [22], [23], [24].

The first model that needs to be pointed out, is the transgenic adenocarcinoma of the mouse prostate (TRAMP) model, which spontaneously induces most mice to develop prostate adenocarcinomas by the age of 12 weeks. Upon castration, 80% of host mice displayed poorly differentiated tumor cells with NE features by another 12-week time period (age of 24 weeks).

These NEPC cells show little to no AR expression and tested positive for neuroendocrine marker SYP, which were AR(+) and SYP(-) before, in early disease stage. However, all TRAMP mice will eventually advance to NEPC, also lacking castration, so consequently, more studies have to be evaluated [22].
The second trace of evidence that supports the transdifferentiation hypotheses, was investigated in LTL331/LTL331R patient-derived xenograft (PDX) model. LTL311 tissue stems from ADT-naive prostate adenocarcinoma and expresses PSA and AR. After host castration, both PSA and AR levels were drastically reduced. Interestingly, several months later a tumor growth reoccurred, which could be defined as CRPC (LTL331R tissue). These tumor cells express several NE markers, such as SYP and CHGA, and furthermore lack AR and PSA expression. Patient-derived xenograft LTL331R tissue was regrafted, into either fully castrated hosts or testosterone-supplemented hosts. The LTL331R tissue maintained a neuroendocrine phenotype and androgen-independent tumor growth. These results indicate an irreversible transition of lineage, demonstrating that ADT triggers adenocarcinoma cells to undergo neuroendocrine differentiation [23].
In a third study, human prostate cancer tissue was examined to further find proof of concept for the transdifferentiation hypotheses. The genome of human prostate biopsies was analyzed and showed very frequent fusion of genes *TMPRSS2* and *ERG* in around 50% of reviewed NEPC tissue, which is the same percentage as in adenocarcinoma. This gene fusion was not detected in normal neuroendocrine cells of the prostate. Another concordance showing relations between adenocarcinoma and NEPC was detected in allelic imbalance analyses of prostatectomy tissue, having identical allelic profiles, but not resembling the profile of non-cancerous NE cells [24].

### 1.2.4 Molecular mechanisms of neuroendocrine prostate cancer

The molecular mechanisms underlying neuroendocrine transdifferentiation are still poorly understood, although mounting evidence suggests a role for genetic, epigenetic, and transcriptomic alteration in several pathways [14].
Very noticeable genomic alterations are Rb1 loss and p53 mutation or deletion in NEPC compared to adenocarcinomas. These findings were observed in whole-exome sequencing data of surgically removed biopsies [25]. Furthermore, *in vivo* mouse studies showed, that the functional loss of *Rb1* facilitates metastasis followed by lineage plasticity of prostate cancer. TP53 depletion accounted for ADT-resistance which resulted in AR-indifferent cell status [26], [27]. In another mouse model, it was demonstrated that Myelocytomatosis (*MYC*) overexpression favors PC to develop various aggressive morphologies, including neuroendocrine PC. MYC protein is a developmental transcription factor that binds to promoter regions of Synaptophysin (*SYP)* and AR. These relationships indicate causal interaction between *MYC* and neuroendocrine differentiation [28].
Tissue-specific gene expression patterns, which establish cell identity are partly regulated by epigenetic mechanisms such as chromatin modification and remodeling. The epigenetic regulator enhancer of zeste homologue (*EZH2*) has been reported to be upregulated in clinical

NEPC biopsies and has been validated in NEPC mouse studies [29]. A remarkable finding was discovered in a genetically modified NEPC mouse model, that reversed NE transdifferentiation by inhibiting EZH2. In this study, AR expression was restored and the sensitivity to enzalutamide was regained. Furthermore, it was determined that EZH2 directly interacts with MYC to inhibit AR-signaling and enhance neuroendocrine expansion [28], [30].
Transcription factors (TF) present in specific combinations induce cell reprogramming and plasticity [14]. Several TFs impacting neuroendocrine lineage have been reported such as Sex determining Region Y-box 2 (SOX2), POU Class 3 Homeobox 2 (POU3F2), Forkhead-Box-Protein A2 (FOXA2), One Cut Homeobox 2 (ONECUT2), Achaete-scute Family bHLH Transcription Factor 1 (ASCL1), Pancreatic and Duodenal Homeobox 1 (PDX1), E2F Transcription Factor 1 (E2F1), Neurogenic Differentiation 1 (NEUROD1) [14], [21], [24], [31]. SOX2 is known to be one of the key transcription factors that play an essential role in maintaining pluripotency as well as guiding neuron precursor cells in proliferation and differentiation. In LNCaP-AR cell culture, neuroendocrine-specific markers (SYP, CHGA) are increased in expression, when either *SOX2* is upregulated or *Rb1* and/or *TP53* are knocked down. The explicit relation of *SOX2*, *Rb1* and *TP53* in association with NEPC is still not well known and needs to be investigated in the future [29]. Puca *et al.* were able to show *DLL3* upregulation in 57.8% of NEPC patients from CTC analysis. Furthermore, the group found that *DLL3* and *ASCL1* are not prominently expressed in localized PC but are highly expressed in non-AR-driven diseases. This feature makes both *DLL3* and *ASCL1* appealing biomarkers and/or possible therapeutic targets. Both named genes are members of the Notch signaling family. Nonetheless, only little is known about the role of Notch signaling in neuroendocrine PC, and more investigation in needed [32].

## 1.3 Circulating tumor cells are molecular signatures of tumor biology

### 1.3.1 Circulating tumor cells display a heterogenous cell population

As discussed previously, metastasis is the most lethal form of prostate cancer resulting in very poor survival of patients [33]. Regardless of significant progress in cancer research, the knowledge of when and how metastasis arises in patients still needs to be investigated more. The fundamental concept of the metastatic cascade is a multi-step process involving the following steps: cancer cell invasion of the primary tumor, intravasation into the bloodstream, survival in blood circulation, and extravasation at the secondary tumor site (Figure 4) [33]. This process is guided by circulating tumor cells (CTCs), which were first reported as “some cells” similar to primary tumor cells, in the blood of a metastatic cancer patient in 1869 [34]. Today it is known that CTCs stem from the primary tumor site, nonetheless, they display a separate cell population [35].

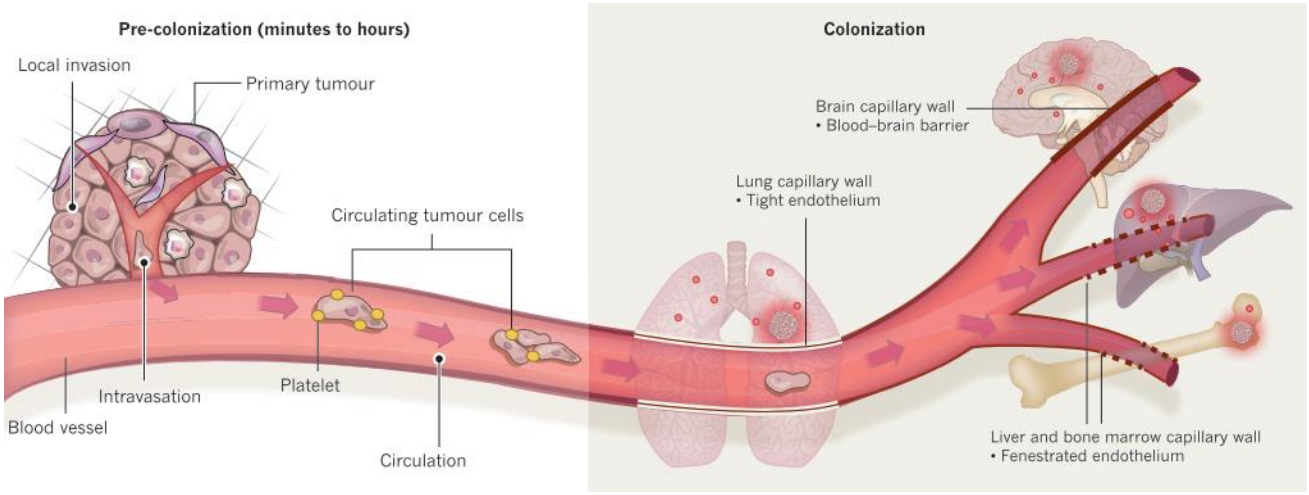


Figure 4: The process of metastatic colonization. Circulating tumor cells intravasate from the primary tumor site into the bloodstream. During transit, CTCs are protected by platelets and sometimes cluster together. The circulatory system moves blood through the lungs and onto other organs, such as the brain, the liver, or bone marrow. CTCs can disseminate in distant locations and extravasate into the target organ. This colonization process develops in many steps and can take years to occur [36].

In malignant disease progression, epithelial tumor cells undergo epithelial-to-mesenchymal (EMT) transition, which contributes to the generation of CTCs. In EMT, cell characteristics shift from an epithelial-to-mesenchymal phenotype, which transforms cell physiological features into a pathological state [37].
In the past, CTC counts have been used by Oncologists as a treatment response indicator and as early detection or disease monitoring tool [38], [39], [40]. Correlations between CTC numbers and disease outcomes have been reported, nonetheless, CTC quantification alone is not a reliable parameter for clinical decision-making. These findings have led to a shift in research to the qualitative analysis of molecular signatures [41], [42].
The most common biomarker applied in CTC characterization is epithelial cell adhesion molecule (EpCAM), since most cancers stem from an epithelial origin. EpCAM expression is very high in prostate cancer and has been used as a metastatic progression prediction tool. However, applying EpCAM as a CTC biomarker has a significant limitation, since CTCs are an immensely heterogeneous cell family with different molecular characteristics in their subpopulations. Heterogeneity in one patient can transpire as a result of EMT [41].

In the field of prostate cancer research, Miyamoto *et al.* have established several blood-based biomarker tests from prostate-derived transcripts. The research group of Dr. Miyamoto has introduced highly specific assays from noninvasive liquid biopsies for localized and metastatic prostate cancer patients. In this study, high expression of androgen receipt splice variant 7 (AR-V7) has predicted resistance to abiraterone and enzalutamide [43].
Abiraterone is an androgen biosynthesis inhibitor, while enzalutamide is an androgen receptor inhibitor, both being used as therapeutics in metastatic prostate cancer patients [13].

## 1.4 Circulating tumor cell isolation techniques

### 1.4.1 Current methods and challenges in CTC enrichment

CTCs shed from primary or metastatic tumor sites into the vascular system. Depending on the cancer type, stage, or previous treatment, their occurrence varies. A reviewed fact is, that CTCs are extremely rare cells but are believed to enrich during disease progression. In most metastatic prostate cancer patients, 10 or fewer CTCs are found in 1 mL of peripheral blood. In contrast, 1 mL of blood also contains 1 million white blood cells (WBC) and even 1 billion red blood cells (RBC) (Figure 5) [44].

In the past, two groups of CTC enrichment technologies have been introduced: Immunocapture methods and methods using biophysical properties for positive selection. Since CTCs display a very heterogenous cell population, methods based on size exclusion, such as membrane filter methods, microfluidics, and density-based methods have shown a volatile recovery rate [45].

To date, only one CTC enrichment method, CellSearch (Menarini Silicon Biosystems), has been approved by the US Food and Drug Administration (FDA). CellSearch was introduced in 2004 and has been a valuable commercial technology used clinically. CTC enumeration has been applied as a prognostic tool that assisted in forecasting survival time in cancer patients [46].

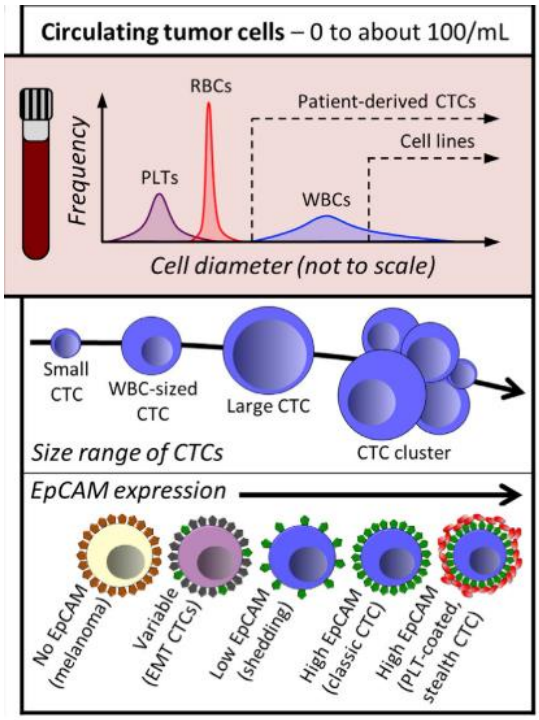


Figure 5: Characteristics of circulating tumor cells. Graphic of frequency and size differences of CTCs and other blood components such as platelets, red blood cells, and white blood cells. Circulating tumor cells are a heterogenous cell population with different expression levels of the epithelial marker EpCAM [47].

CellSearch is an immunomagnetic capture method that uses anti-EpCAM-coated magnetic beads to bind to CTCs. Labeled CTCs are then isolated by magnetic-activated cell sorting (MACS). Additionally, in-device immunostaining for cancer cell markers cytokeratin (CK) -8,-18, -19, as well as staining for the leukocyte marker CD45 is performed. Afterward, fluorescence imaging is used to verify circulating tumor cells [45].
One major shortcoming of immunocapture methods, including CellSearch, is that most methods are based on EpCAM expression. As previously discussed, it is widely acknowledged, that CTCs undergo EMT, and thereof often lose epithelial characteristics. Mesenchymal CTCs have been reported to display an aggressive metastatic potential than their fellow epithelial CTCs. As a consequence of this data, CTC enrichment methods based on EpCAM expression alone can deliver an unreliable CTC number, because the nature of CTC heterogeneity has not been taken into consideration [48].
To overcome this limitation, microfluidic technologies and immunocapture have been combined into a multistep purification method [45].

### 1.4.2 Microfluidic immunocapture combined with size exclusion provides a solution for circulating tumor cell isolation

The research group of Dr. Mehmet Toner has introduced a CTC isolation strategy, the CTC-iChip 2.0, which is based on the depletion of hematopoietic cells. The CTC-iChip 2.0 is a high-throughput monolithic chip made of medical-grade cyclic olefin copolymer (COC) and is manufactured by utilizing laser and thermal injection-compression molding (Figure 6.A). The symmetrical architecture of the chip is able to incorporate five microfluidic stages, to separate CTCs, into one device [49], [50], [51]. The chronological order of the microfluidic separation stages is implemented in: non-equilibrium inertia separation array (NISA), inertial focusing 1 (IF), magnetically-activated cell sorting 1 (MACS), inertial focusing 2, and magnetically-activated cell sorting 2 [47].
Whole blood of cancer patients is incubated with a biotinylated CD45, CD16, and CD66b antibodies and streptavidin magnetic beads, targeting surface antigens of white blood cells. The blood sample enters the chip at an inlet and flows through a filter (90µm→60µm→45µm→35µm pore size) to break up eventually coagulated cells.
The first stage of separation, NISA, combines inertial focusing with repetitive flow-shifting (Figure 6.B, Part 2). The applied pressure in the chip lets cells bump on the rectangular islands in NISA, and cell flow focuses small cells in the lower exit lane. Red blood cells, platelets, and plasma proteins are siphoned, and all larger cells remain in the buffer co-flow channel (Figure 6B, blue arrows flow). The next stage is inertial cell focusing, in which cells are aligned by three hydrodynamic forces: wall interaction force, gradient lift force, and a drag force resulting from a secondary flow (Figure 6.B, Part 4).
The focused cells are released in a wider channel, where consequently, flow speed is decreased before they enter the first magnetic field region. The magnetically labeled white blood cells are gathered in the center of the channel by the magnetic flux gradient (200 T/m) going into the waste department (Figure 6.B, Part 5). WBC-bead complexes being focused in

the center prevents plaque formation close to the walls, where lower shear zones are located. MACS1 stage separated WBCs labeled with 6 or more magnetic beads.

The remaining cell flow access the second phase of inertial focusing channels (Figure 6.B, Part 7). Afterward, the cells pass through the second MACS stage (Figure 6.B, Part 8), which has a magnetic flux gradient of 425 T/m, that is able to remove WBCs labeled with at least 1 magnetic bead.

After both MACS steps 99,9% of leukocytes have been depleted from the blood sample and unlabeled CTCs proceed toward the product output [51], [47]. Some notable advantages of the CTC-iChip technology are firstly its fast processing time of 10mL/h and secondly, the negative enrichment mechanism that allows for separation of CTCs with independent cell surface marker expression [51].

To summarize, obtaining viable CTCs by microfluidic isolation with the CTC-iChip 2.0 can enable a wide range of possibilities in NEPC research. Utilizing the knowledge of molecular signatures of CTCs, will aid noninvasive blood sampling, *in vitro* drug testing and can guide personalized medicine.

Abbreviations:
CTC circulating tumor cell, WBC white blood cell, NISA non-equilibrium inertia separation array

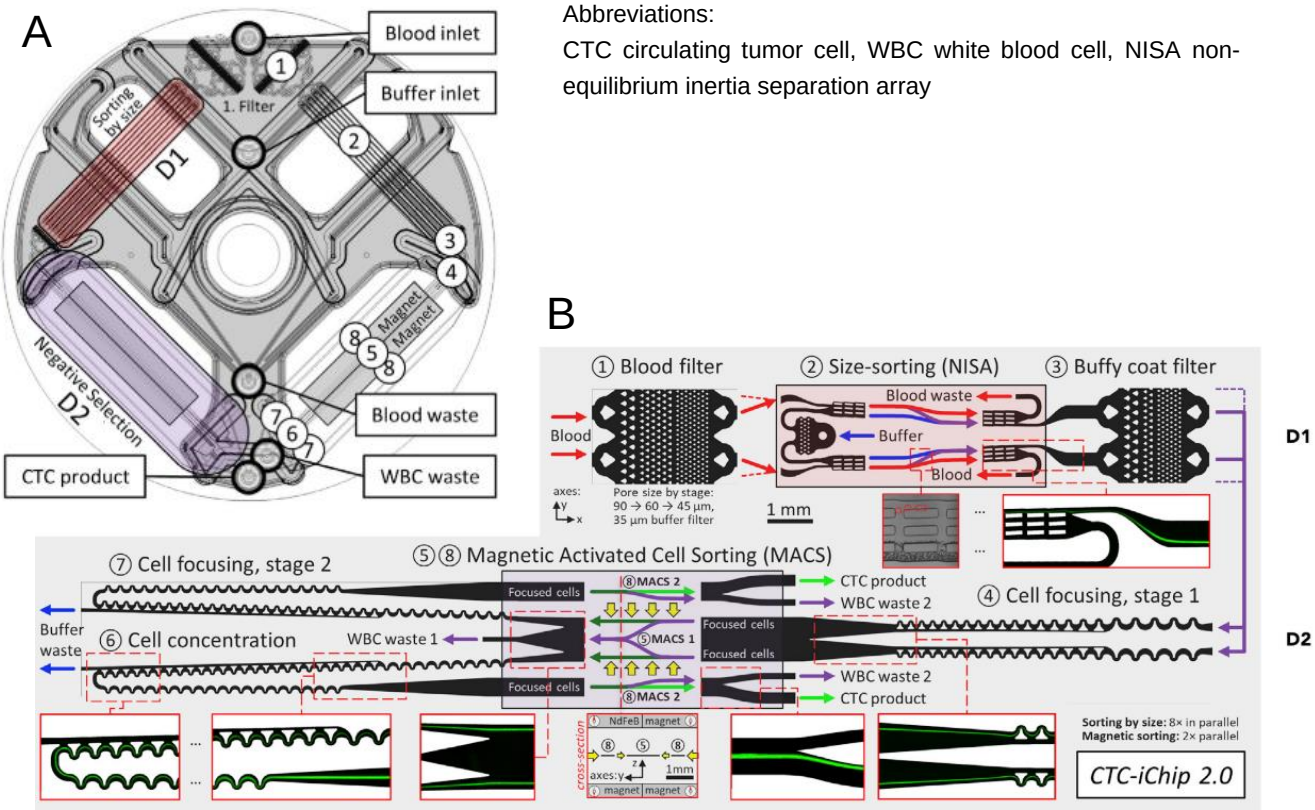


Figure 6: The CTC-iChip 2.0 technology. (A) The iChip is produced in bilateral symmetry. Two stages of size sorting (D1) and negative selection (D2) are implemented. The five tube in- and outlets (blood inlet, buffer inlet, blood waste, WBC waste, CTC product) for liquids are depicted in the graphic. (B) Patient blood is processed in eight consecutive microfluidic steps (1-8) [47].

## 1.5 Transcriptional downstream analysis of circulating tumor cells gives insights into molecular features of neuroendocrine prostate cancer

Prostate cancer has remained the second most common cause of cancer death in adult men in 2021 [1]. As a result of androgen deprivation therapy, the variable biological behavior of prostate cancer cells displays a challenge in finding the optimal management for patients [10], [11]. Traditionally, surgical biopsies at metastatic sites, have given information on disease progression and on clinical decision-making. Furthermore, biopsies are tedious and painful to repeat. In contrast, liquid biopsies, which are defined as the analysis of bodily fluids such as blood or urine samples, are easy to repeat and a minimal inconvenience for the patient. Liquid biopsies analyzing circulating tumor cells, extracellular vesicles, and circulating tumor DNA or RNA, have been shown to be a powerful tool in the management of prostate cancer [52].

To get information on prostate tumor molecular signatures derived from CTCs, digital droplet polymerase chain reaction (ddPCR) has shown to be an attractive method, in the field of clinical precision oncology. ddPCR provides the absolute quantification of its nucleic acid target sequences with high-precision and can be applied to clinical and research diagnostic purposes [53]. This digital method uses hydrolysis probes labeled with reporter fluorophores (such as FAM and HEX), in a similar manner as in preparation of real-time PCR reactions [54].

The by far most widely applied ddPCR platform is the one introduced by Bio-Rad (Bio-Rad, Hercules, California, USA) in 2011 [55], [56]. A ddPCR workflow (Figure 7A) has several steps, starting with pipetting the PCR reaction including the to-be-analyzed- sample, primer and probes, and ddPCR master mix together in a 96-well PCR plate (Figure 7A&B, Part 1). Afterward, this plate is placed in a fully automated droplet generator (AutoDG Droplet Digital PCR System, Bio-Rad) [53]. The droplet generator partitions the PCR reaction into around 20.000 nanoliter-sized individual reaction vessels, which are aqueous droplets encapsuled by oil, in a new 96-well plate (Figure 7A&B, Part 2). In the partitioning process, the sample is distributed in droplets, which either contain or do not contain a target sequence. This enables many independent PCR sub-reactions in which, afterward, target amplification takes place in the thermocycler (Figure 7A&B, Part 3) [53], [57].
After PCR, the fluorescence signal of the portion of positively amplified target sequences is measured via end-point quantification corrected by Poisson's statistics (Figure 7A&B, Part 4) [56]. With help of the Poisson distribution, sample concentration is estimated with the formula: copies per droplet = – ln (1 – fraction of positive droplets [56], [57]. Although ddPCR is a digital method, the fluorescence signal is initially detected analog, so a threshold needs to be applied, to distinguish positive droplets from negative background signal. The digital signal readout of target concentration is available via Software output (Figure 7A&B, Part 5) [58].

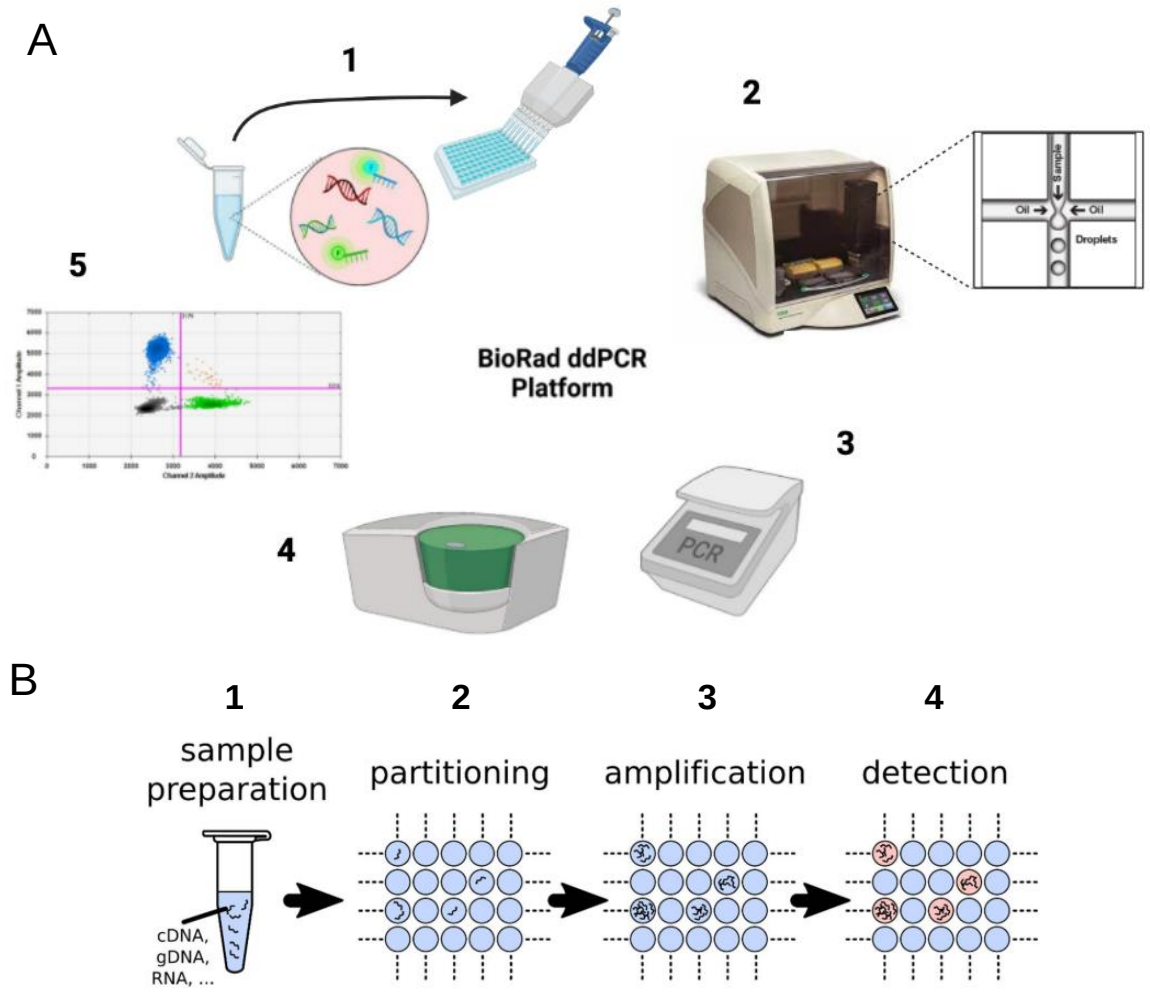


Figure 7: (A) BioRad ddPCR platform with corresponding instruments. (1) All reagents, including the sample, are pipetted in a 96-well plate. (2) The droplet generator (AutoDG) creates around 20.000 nanoliter-sized reaction vessels. (3) In a thermocycler, the target amplification takes place. (4) Every droplet is analyzed in the droplet reader. (5) The software gives information on the readout of every single sample. Figure adapted with BioRender.com from Olmedillas-López *et al* [53]. (B) Events in the droplets in ddPCR. (1) The sample is prepared by adding ddPCR master mix and probers and probes. (2) In an automated process, the droplets are generated. Some droplets contain the target sequence, some do not. (3) In PCR reaction the target nucleic acid is amplified. (4) The fluorescence of the target is measured by absolute quantification. Figure taken from Quan *et al.* [58].

The gold standard method in liquid cancer biopsies has been reverse-transcription quantitative PCR (RT-qPCR). Nonetheless, one major advantage of ddPCR over RT-qPCR is its superior sensitivity (with a limit of detection of one copy of transcript), as well as the capability to measure absolute quantification without a standard curve [59]. Standard curve-independent quantification gives highly reproducible data. Another advantage of ddPCR technology is, that it can measure extremely low target concentrations in clinical prostate cancer patients [58].
As described before, in chapter 1.2.4, the molecular biology of neuroendocrine prostate cancer is not entirely controlled by mutations in DNA, but rather the result of both genetic and

epigenetic changes. Monitoring the changes in RNA expression by ddPCR is, therefore a powerful tool in translational oncology, giving physicians information on response to treatment and observing for development of resistance. The discovery of new biomarkers in CTCs could improve the informative value of liquid biopsies. Summing up the results obtained from liquid biopsies and from immunohistochemical evaluation of PC biopsies, can contribute significantly to PC care in the coming years [52].

## 1.6 Aims

In this thesis, we will investigate the highly clinically relevant problem of neuroendocrine (NE) transdifferentiation in prostate cancer. The improved molecular understanding of NE transdifferentiation in prostate cancer patients represents an unmet need that would have a significant impact on the clinical management of metastatic disease.

As previously mentioned, the molecular signatures of neuroendocrine prostate cancer are still a subject of debate. As discussed in chapters 1.2.3 and 1.2.4, there is underlying evidence of various regulatory and signature NE hallmark genes. In this thesis, a selection of possible NE biomarkers will be evaluated on a transcriptional level. Taking the heterogeneity nature of CTCs into consideration, 15 different markers will be tested for specificity and sensitivity. A selected, minimized panel of targets will first be evaluated in healthy donor samples that are spiked with cancer cell line cells. Secondly, the assay will be applied to CTC signatures of metastatic cancer patients.

The overall research agenda is the utilization of a microfluidic chip (CTC-iChip 2.0) to isolate circulating tumor cells (CTCs) from a simple blood draw from prostate cancer patients to evaluate CTC subsets for hallmarks of neuroendocrine phenotype.

The main goal of this thesis is to identify neuroendocrine hallmark genes, that will be investigated by RNA-based assays and hopefully can be utilized as reliable biomarkers.

Table 1: Selection of regulatory genes of neuroendocrine transdifferentiation in prostate cancer.

| Abbreviation | Gene |
|---|---|
| DLL3 | Delta-like 3 |
| EZH2 | Enhancer of Zeste Homolog 2 |
| MYC | Myelocytomatosis |
| SYP | Synaphtophysin |
| CHGA | Chromogranin-A |
| CSPG4 | Chondroitin Sulfate Proteoglycan 4 |
| FOXA2 | Forkhead-Box-Protein A2 |
| NEUROD1 | Neurogenic Differentiation 1 |
| POU3F2 | POU Class 3 Homeobox 2 |
| SOX2 | Sex determining Region Y-box 2 |
| ASCL1 | Achaete-scute Family bHLH Transcription Factor 1 |

| | |
|---|---|
| PDX1 | Pancreatic and Duodenal Homeobox 1 |
| E2F1 | E2F Transcription Factor 1 |
| ONECUT2 | One Cut Homeobox 2 |
| TACSTD2 | Tumor Associated Calcium Signal Transducer 2 |

# 2 Material and Methods

## 2.1 Cell culture of neuroendocrine gene-carrying cancer cell lines used as positive control template and spike-in cells

mRNA expression data found in the Cancer Cell Line Encyclopedia (CCLE) established by Broad Institute identified the cell lines PC3, VCaP, LNCaP, 22RV1, HOP62 and NCI-H727 as combined carriers of all 15 genes which we will investigate. The prostate cancer cell lines, PC3, VCap, LNCap, and 22RV1, and the lung cancer cell lines, HOP62, and NCI-H727, are carrier of various of the to-be-investigated neuroendocrine genes with different expression levels. (Further details can be found in the results section 3.1).

The named cell lines were obtained from the American Type Culture Collection (ATCC) and cultured in their recommended media (Gibco) (Table 2) at adherent conditions at 37°C with 5% $CO_2$. All cell media was supplemented with 10% fetal calf serum (FCS) (Gibco) and 1% penicillin/streptomycin (Gibco). The prostate cancer cell lines were passaged 1:3 every seven days. Lung cancer cell lines were passaged 1:4 every three to four days. Cell lines were used for experiments until passage 18.

Table 2: The listed cell lines were used in culture to isolate RNA from and further study the neuroendocrine phenotype of prostate cancer. Information is taken from ATCC.

| Cell line | Lineage | Culture media |
|---|---|---|
| PC3 | Prostate Cancer | F-12 K |
| VCap | Prostate Cancer | RPMI-1640 |
| LNCaP | Prostate Cancer | RPMI-1640 |
| 22RV1 | Prostate Cancer | RPMI-1640 |
| HOP62 | Lung Cancer | RPMI-1640 |
| NCI-H727 | Lung Cancer | RPMI-1640 |

## 2.2 Automated cell sorting to obtain single cells for spike-in samples

The cell line NCI-H727 is a carrier of all eight genes (DLL3, EZH2, MYC, SYP, CHGA, NEUROD1, E2F1, and PDX1) which were investigated as possible neuroendocrine biomarkers. These findings were determined by analysis of the CCLE database. Further information on the selection of the genes can be found in the results chapter 3.2.

In order to mimic the behavior of prostate cancer patient samples, containing single CTCs, spike-in samples were prepared. The spike-in samples contained 20 mL of healthy donor blood, which was split into five fractions. To each fraction of blood, a number (0, 1, 3, 5, 10) of NCI-H727 cells was added.
NCI-H727 cells at 70% confluency were trypsinized and prepared in 1 mL cold PBS (Phosphate-buffered saline) (Gibco) with 1% FCS (Gibco). From this suspension, single cells were picked by fluorescence-activated cell scanning and transferred into a new sample tube (15 mL falcon) filled with 300µL cold PBS by using the automated Sony cell sorter (Sony SH800S). The instrument was used in the automatic setup process, which included the steps of chip alignment (100µm chip), droplet calibration, side stream calibration, and sort delay calibration.
After calibration, a polygon on the light scatter plot was drawn to select single cells for sorting. A series of single cells (0, 1, 3, 5, 10) were placed in separate tubes and one-fifth of the male healthy donor blood was aliquoted into each sample. The spiked samples were then processed using the CTC-iChip 2.0 as described below.

## 2.3 Microfluidic cell isolation

The negative-selection method to capture CTCs described below, has several steps to obtain an as pure as possible CTC product. Firstly, the blood samples, of around 20 mL, (patient or healthy donor samples) must be prepared, and secondly, the CTC-iChip tower must be assembled before the blood can be run through the chip. The last step is to store the CTC product and clean the CTC tower to be available for the following sample.
Blood samples were placed on the rotator, immediately after acquisition so that clotting will be prevented. All samples were processed in the next four hours of drawing.

Before the blood sample, healthy donor / spike-in / patient sample, could be handled, the custom-made running platform had to be fully assembled. The instrument's power was turned on, and the door (Figure 8.A, Part 1) must be opened to insert a new CTC-iChip 2.0. All tubing was fixed in place, and the door was locked. All valves can be opened/closed manually, if the platform is not used in automated mode, with buttons placed on the control unit (Figure 8.A, Part 2). The top right line was connected to a Luer adapter that was wrenched in the buffer cartridge (Figure 8.A, Part 3). The buffer cartridge was filled with 350 mL running buffer (preparation described in chapter 2.3.1), and the lid was placed on and locked. When pressing the “prime” button the system got pressurized to 48.0 psi, and buffer wet and primed the whole chip and tubing. Priming the chip takes around 10 minutes and afterward, the chip’s top line was connected to the sample tube (Figure 8.A, Part 4). The chip's right-most and left-most bottom lines were connected to waste bags (Figure 8.A, Part 5, 6). The middle output line was placed in a labeled 15 mL falcon tube, sealed with a parafilm, and secured in the product tube holder (Figure 8.A, Part 7). This secured falcon tube was stored on ice, during sample processing.

A very crucial step before loading the sample is to check the magnet alignment in the tower. The alignment can be checked by looking through the door with a magnifying glass. The main aim of the process is to align the center of the deflection channel to the line, where two magnetic sticks meet (Figure 8.B). In this channel, the magnetic field is 0. The magnets can be moved manually by turning the knobs on the door lock (Figure 8.A, Part 8).
Misalignment will cause the carryover of other blood components to the product, which leads to undesired contamination.

A

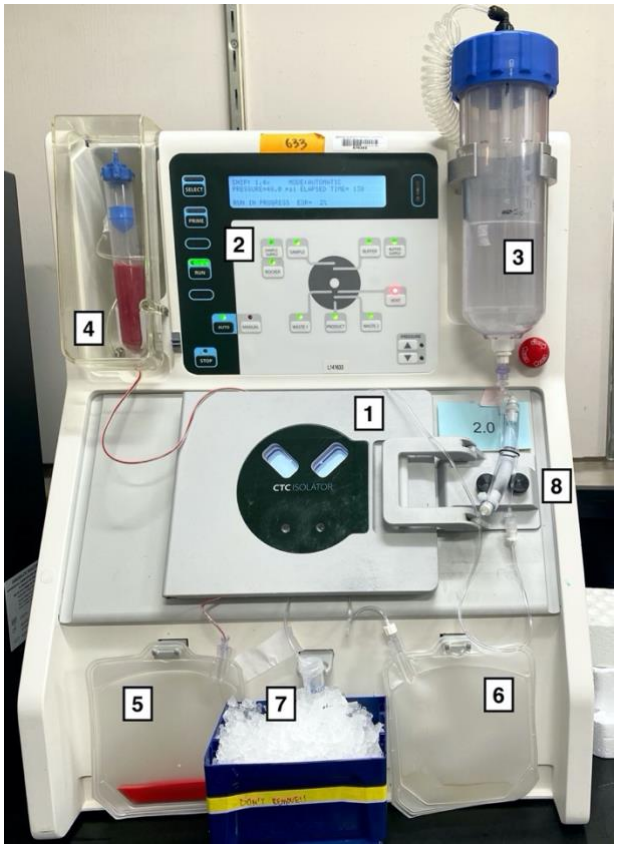


B

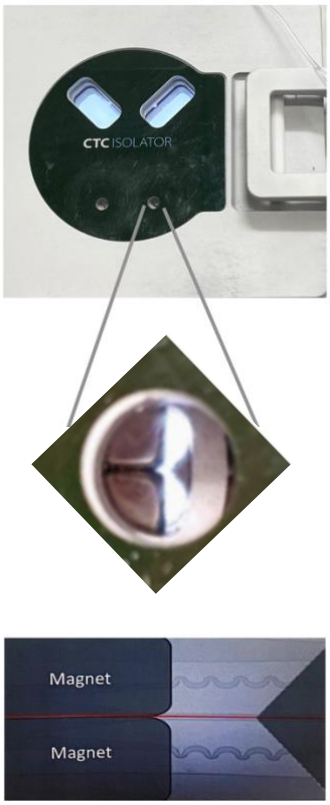


Figure 8: (A) The CTC-iChip tower platform setup in operation. Around 20 mL of patient blood is being processed. Part numbers are shown in black squares and referenced in the methods section described in the paragraph below. (B) Close-up of the microfluidic chip fixed in place in the running platform. Successful chip alignment can be checked visually, when looking through the door with a magnifying glass. The middle of the magnets must be aligned with the center of the deflection channel (red line) and the tip of the alignment marker (dark grey triangle).

In the meantime of tower assembling and priming, the blood sample was prepared (Figure 9). The preparation of all reagents used is described in the next chapter “Microfluidic processing Material preparation”.
In total, 14 patient, 5 healthy donor, and 5 spike-in samples were processed in this project. First, the individual blood sample was placed in a 50 mL falcon tube and incubated on the tube

rotator for 30 minutes with an appropriate amount of antibody cocktail (18 µL AB cocktail per mL of blood). Antibody preparation is described in chapter 2.3.1.
Second, the blood was spiked with 120 µL magnetic bead per mL blood and placed on the tube rotator for another 20 minutes. A critical step is to vortex the magnetic meads, at around 2000 rpm for 1 min, before adding them to the blood, so the suspension is homogenous, and the beads do not clump together.
After the second incubation step the blood sample was carefully poured into the sample tube (Figure 8.A, Part 4). The sample was diluted by adding an appropriate amount of buffer to the blood. The amount of buffer was calculated by taking the mL of blood and subtracting the bead and AB volumes combined. Once the sample holder was closed with a plastic cap the “Run” button on the control unit tube (Figure 8.A, Part 2) can be pressed. This activates the pressurizing of the system and once process pressure was reached, the sample and buffer got pushed through the channels of the chip.
After the procedure was finished the remaining buffer was drained, the tower was dissembled and the used chip, waste bags, sample tube and buffer cartridge were disposed. The final product, containing patient-derived CTCS, or spiked-in NCI-H727 cells, in the 15 mL falcon tube was centrifuged at 4550 x g for 5 minutes. The supernatant was discarded, and 200 µL RNAlater (Thermo Fisher Scientific) were pipetted on the isolated cells. The product was flash-frozen in liquid nitrogen and stored at -80°C until further downstream processing.

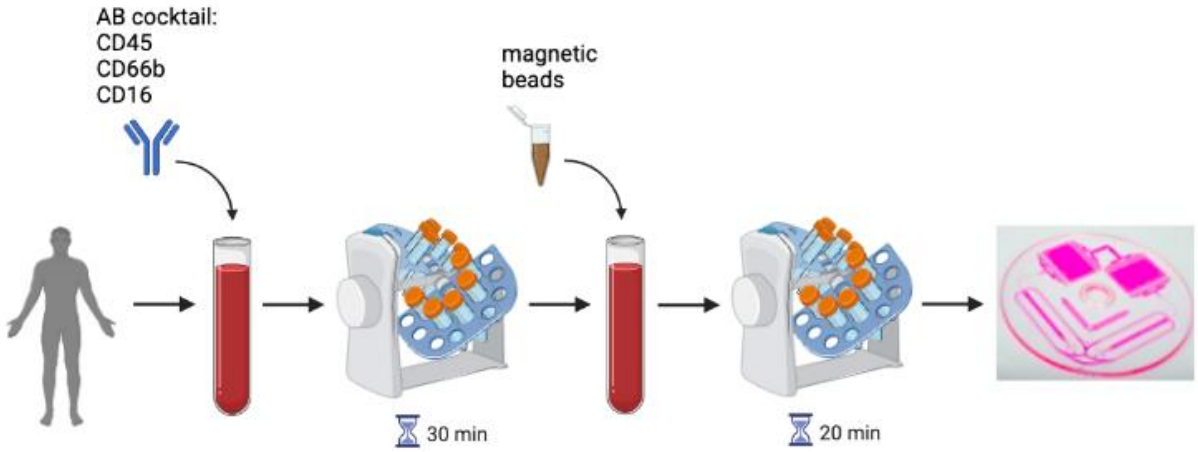


Figure 9: Blood preparation and incubation for microfluidic processing. After obtaining blood from a prostate cancer patient, the blood was processed in the course of four hours. The blood was spiked with two different reagents (Antibody cocktail and magnetic beads) to achieve the separation of CTCs from whole blood. The graphic was created with the help of Biorender.com.

## 2.3.1 Microfluidic processing material preparation

The following reagents were prepared on the day before blood processing or stored until referenced shelf-life periods.

To prepare the running buffer, 5 g of Kolliphor P188 (Pluronic-F68) (Sigma Aldrich) were added into 500 mL of 1 x PBS (Gibco) for a final 1% concentration. To dissolve the crystals, the mixture was placed on a rocker at low speed for 20 minutes. The buffer was filtered through a 0.2 µm pore size Nalgene filter system (Thermo Fisher Scientific). The buffer can be stored for 2 weeks upon preparation date at ambient temperature.
The AB cocktail contained a 10:1:1 ratio of biotinylated CD45, CD66b and CD16 antibodies. The following ABs were used: CD45 Monoclonal Biotin-Clone HI30 (Invitrogen), CD16 Monoclonal Clone 3GB (BD Bioscience), CD66b Monoclonal Clone 80H3 - (Novus Biologicals). AB cocktail was made on demand and could be stored for one week.
For our experiments, the Invitrogen Dynabeads MyOne Streptavidin T1 were used. The purchased bottle was vortexed very well before aliquoting 10 mL in a 15 mL falcon tube. The tube was placed on a magnetic holder until the solution was clear and all beads were magnetically attracted to one wall of the tube. The supernatant, containing 1 x PBS, was discarded, and the beads were washed three times with filtered 0.01% Tween 20 (Sigma Aldrich) in PBS and finally resuspended in 0.1% BSA (Sigma Aldrich). Finally, the resuspended beads were vortexed, and 1 mL aliquots were pipetted in 1.5 mL Eppendorf tubes for storage for up to 4 weeks at 4°C During all the wash steps the falcon tube was located in the magnet, so bead disruption was prevented.

## 2.4 Downstream processing

### 2.4.1 RNA isolation

All RNA isolation protocols were conducted in an RNA-free environment. For cell lines, healthy donor spike-in samples, and patient samples RNA extraction, the Qiagen RNeasy Micro Kit was used with an adapted protocol.

Cell lines and microfluidic processed blood samples have slightly different starting steps for the isolation protocol. The procedure for cell lines will be described first and the procedure for all blood samples second.

NCI-H727 cells were grown in culture dishes (10 cm diameter) until they were 80-90% confluent. All media was removed before starting the RNA isolation procedure. To harvest the cells and disrupt the plasma membrane, every dish was treated with 350 µL RLT lysis buffer, also containing 1% β-Mercaptoethanol. This lysate-buffer mixture was collected with a cell scraper, pipetted into a QIAshredder spin column, and centrifuged at 2100 x g for 1 minute. As the lysate goes through the spin column membrane, it is evenly homogenized.
The frozen samples that stemmed from microfluidic processed blood samples were thawn and reconstituted in 350 µL RLT lysis buffer with 1% β-Mercaptoethanol. The tube was vortexed at centrifuged at 1000 x g for 1 minute.

From this point on, cell line and blood samples have the same following isolation steps. The liquid was then mixed with 350 µL of 70% Ethanol by pipetting and transferred to an RNeasy

MinElute spin column. The cell sample was then lysed in Guanidine-thiocyanate-containing buffer (RLT buffer) combined with Ethanol, which allows for selective RNA binding to the RNeasy MinElute membrane. After centrifugation at 10 000 x g for 30 seconds the flow through was discarded. Residual DNA was removed by adding DNase I stock solution (10 µL) in RDD Buffer (70 µL) and incubating the DNase mix on the membrane for 15 minutes. Any contaminants were removed by several washing steps. The first one was done by adding 350 µL RW1 Buffer and centrifuging it for 30 seconds at 10 000 x g. The collection tube including the flow though was discarded and the spin column was placed in a new collection tube. The second step was washing the membrane with 500 µL RPE Buffer. The sample was again centrifuged 30 seconds at 10 000 x g. The flow through was discarded and the final wash was performed by adding 500 µL of 50% Ethanol. The collection tube, which held the flow through, was removed and the spin column was placed in a new 2 mL collection tube. For obtaining a high RNA yield, the spin column membrane was dried by 5 minutes of centrifugation at 21 000 x g. The spin column was set in a 1.5 mL Eppendorf tube and 14 µL RNase-free water was pipetted directly in the center of the membrane. To isolate the RNA the column was centrifuged at 21 000 x g for 1 minute. The eluted RNA concentration was measured via Nano Drop (Thermo Scientific) and diluted to 100 ng/µL. These RNA samples were further reverse transcribed to cDNA for ddPCR analysis.

#### 2.4.1.1 Reverse transcription of cDNA from cell lines

The single-stranded cell line RNA was reverse transcribed (RT) to cDNA by using the SuperScript III First-Strand Synthesis SuperMix Kit (Invitrogen). All reagents and samples were kept on ice and the task was performed in an RNase-free environment. Each solution, except Enzyme Mix, was mixed by gentle vortexing. A Master Mix (MM), composed of RT Reaction Mix and Enzyme Mix, was prepared for all reactions (Table 3).

The 2X RT Reaction Mix includes oligo (dT), random hexamers, $MgCl_2$, and dNTPs in a buffer solution. Oligo (dT)s anneal selectively to the poly-(A)-tail of mRNA templates. One reaction contained 10 µL 2X RT Reaction Mix, 2 µL Enzyme Mix and 8 µL input RNA (100 ng/µL). The RT PCR reactions were pipetted in a 0.2 mL PCR grade tube and vortexed before placing the tubes in the thermocycler (Bio-Rad C1000 Touch Thermal Cycler). The mixture was incubated at 25°C for 10 minutes. cDNA synthesis was performed by incubating the tubes for 30 minutes at 50°C. The reaction was stopped by heating to 85°C for 5 minutes. To remove the mRNA template from the newly synthesized cDNA, 1 µL of *E.coli* RNase H was added and incubated at 37°C for 20 minutes.

After completing the cycling program, the samples remained in the cycler at 4°C. The sample concentration was measured by using a NanoDrop spectrometer (Thermo Fisher Scientific). Afterward, the samples were diluted to 1 ng/µL before they were snap-frozen in liquid nitrogen and stored at -20°C.

Table 3: Qiagen Reagents used for 1 reaction of reverse transcription.

| Reagent | 1 rxn |
|---|---|
| 2X RT Reaction Miix | 10.0 µL |
| RT Enzyme Mix | 2.0 µL |
| RNA | 8.0 µL |
| **Total volume** | **20 µL** |

#### 2.4.1.2 Blood sample cDNA reverse transcription and amplification of blood samples

All healthy donor, spike-in, and patient RNA samples were processed to double-stranded cDNA by using the SMART-Seq HT Kit (Takara). These blood samples mostly contain very little RNA content, since CTCs or spiked-in cells, are very rare. Consequently, a Kit which amplified nucleic acid content in the process, was used. Nucleic acid content obtained from cell culture (chapter 2.4.1.1) was high enough to skip the amplification step.

The used Kit reagents and RNA samples were always kept on ice.

First, a stock solution containing of 19 µL 10X Lysis Buffer and 1 µL RNase Inhibitor was prepared, which is the appropriate amount for 20 samples. Each isolated RNA template (4.5 µL) was prepared in a 0.2 mL RNase-free PCR tube. Reaction Buffer (1 µL), and nuclease-free water (6 µL) were added to have a total of 11.5 µL in the tube. To bring the volume to 12.5 µL, 1µL of 3' SMART-Seq CDS Primer II A (sequence: AAGCAGTGGTATCAACGCAGAGTACT), was added, and the samples were briefly vortexed and spun down (Table 4).

The samples were incubated at 72°C for 3 minutes in a preheated thermocycler and immediately after placed on ice for 2 minutes. A 1:1 ratio (12.5 µL) of premade Master Mix (Table 5) was added and the cycling program was set to 42°C for 90 minutes, 95°C for 1 minute, 10 cycles of 10 seconds at 98°C, 30 seconds at 65°C, 3 minutes at 68°C and finally 10 minutes at 72°C.

Table 4: Reagents used for reverse transcription reaction.

| Reagent | 1 rxn |
|---|---|
| 10X Reaction Buffer | 1.0 µL |
| Sample RNA | 4.5 µL |
| Nuclease-free water | 6.0 µL |
| 3' SMART-SeqCDS Primer II A | 1.0 µL |
| **Total volume** | **12.5 µL** |

Table 5: Reaction mix for amplification of cDNA templates in 10 cycles.

| **Reagent** | **1 rxn** |
|---|---|
| Nuclease-Free water | 0.7 µL |
| One-Step Buffer | 8.0 µL |
| SMART-Seq HT Oligonucleotide | 1.0 µL |
| RNase Inhibitor | 0.5 µL |
| SeqAmp DNA Polymerase | 0.3 µL |
| SMART Scribe Reverse Transcriptase (100 U/µL) | 2.0 µL |
| **Total volume** | **12.5 µL** |

PCR-amplified cDNA was later purified by immobilization using Agencourt AMPure XP Kit (Beckman Coulter). AMPure XP beads were vortexed very well before adding 25 µL to each sample. The cDNA – beads mixtures were incubated at ambient temperature for 8 minutes before placing them on a magnetic separation device for 6 minutes. A separation between beads and supernatant was visible, and all clear liquid was discarded. Afterward, a wash with 200 µL of 80% Ethanol was performed without disrupting the beads. After 30 seconds, the Ethanol was removed carefully by pipetting. This wash was performed twice. The samples were incubated for 3 minutes at ambient temperature until the beads have dried up. 17 µL of elution buffer was added to cover the bead pellet. All sample tubes were mixed well by vortexing and again incubated at ambient temperature for 2 minutes to rehydrate. The samples were once more placed on the magnet for 1 minute until the solution was completely clear. The supernatant containing purified cDNA was transferred In a low-bind 1.5 mL Eppendorf tube and diluted 1:10 in nuclease-free water. The cDNA was stored at -20°C until further downstream processing.

## 2.4.2 Digital droplet PCR

In general, a workflow for digital droplet PCR has several steps: preparing cDNA, setting up reactions, generating droplets, thermal cycling, and analyzing on the droplet reader.

The ddPCR reaction mixture consisted of 11 µL 2X Supermix for probes (Bio-Rad), 1.1 µL primer/probe assay (forward and reverse primer 900 nM, probe 450 nM) (Table 7), 8.8 µL cDNA template. As a positive and negative control, either 1.1 µL cDNA (1 ng/µL) of a respective gene-carrying cell line, or a non-template control (1.1 µL water) were added to 7.7 µL of water in every experiment. All ddPCR reactions were pipetted in clear ddPCR 96-well plates (Bio-Rad) and sealed at 180°C using the PX1 PCR Plate Sealer (Bio-Rad). The plate was vortexed on every corner for 30 seconds to ensure that all reagents were well mixed and afterward centrifuged at 1000 x g for 1 minute in a table-top centrifuge (Avanti J-15R, Beckman Coulter). This ensured the reactions were at the bottom of the well, and the PCR plate was placed in the block in the automated droplet generator (AutoDG, Bio-Rad). Prior to droplet generation, the AutoDG has been loaded with the appropriate number of cartridges (1 cartridge per each 96-well column) and pipette tips for AutoDG (2 tip columns per 96-well column). An

empty 96-well plate, in which the droplets were generated in, was installed in the cold block in the generator. The samples were emulsified (Oil by Bio-Rad) by the automated system in approximately 20 000 droplets resulting in an end volume of 40 µL. In the process of droplet generation, the surface area of liquid-oil emulsion expands in the well.

Immediately after the droplet generation was completed, the plate was transferred to the thermocycler (C1000 Touch Thermal Cycler, Bio-Rad). Thermal cycling conditions were set to initial denaturation of 95°C for 1 minute, followed by denaturation at 94°C for 30 seconds, annealing at 70°C for 10 seconds, 53°C for 30 seconds, 70°C for 50 seconds and final 98°C for 10 minutes (Table 6). The denaturation, annealing, and elongation steps were performed in 45 cycles.

After PCR amplification, the number of fluorescent positive droplets (FAM-channel) were counted with QX200 droplet reader (Bio-Rad) and data was analyzed using the QuantaSoft software (Version 1.7.4.0917, Bio-Rad). The PCR threshold was set manually. The results readout was quantified by positive and negative droplets. Clinical samples were analyzed in single reactions.

Table 6: ddPCR cycling conditions used for amplification and quantification of cDNA samples.

| Step | Cycles | Temperature | Time |
|---|---|---|---|
| Initial Denaturation | 1 | 95 °C | 10 minutes |
| Denaturation | 45 | 94 °C | 30 seconds |
| Annealing | | 70 °C | 10 seconds |
| Elongation | | 53 °C | 30 seconds |
| | | 70 °C | 50 seconds |
| Final extension / Signal stabilization | 1 | 98 °C | 10 minutes |
| Hold | - | 4 °C | infinite |

Table 7: Neuroendocrine prostate cancer-specific primers and probes used in ddPCR. Custom hydrolysis probes containing a FAM fluorescent dye were ordered at Integrated DNA Technologies (IDT, Iowa, USA). The probes are labeled with a fluorescent reporter at one end, and a quencher of fluorescence at the other end.

| Target Gene | Primer / Probe sequence |
|---|---|
| **DLL3** | Fwd: CAACCTAAGGACGCAGGAG<br>Rev: GTCTACATCTTCAGGGCGATT<br>Probe: ATGGTCCGAGCTCGTCCGTAGATT |
| **EZH2** | Fwd: CATCCAGACTGGCGAAGAG<br>Rev: TCGATGCCGACATACTTCAG<br>Probe: TTACAGATACAGCCAGGCTGATGCC |

| | |
|---|---|
| **MYC** | Fwd: TTCTCTCCGTCCTCGGATT<br>Rev: TTGTTCCTCCTCAGAGTCGCTGC<br>Probe: CAACATCGATTTCTTCCTCATCTTC |
| **SYP** | Fwd: CACCTCCTTCTCCAATCAGATG<br>Rev: GGGTGGAGACCTAGGGTATAG<br>Probe: TAGTCTGGTCAGTGAAGCCCAGGA |
| **CHGA** | Fwd: TCCAGGTCCGAGGCTAC<br>Rev: CTGGTGGGCCACTTTCTC<br>Probe: AGGAGAAGAAAGAGGAGGAGGGCA |
| **CSPG4** | Fwd: TGCTGTGGCTGTGTCTTT<br>Rev: GCCAAGAGATTGGAGGCAT<br>Probe: AGCCACCTCTGGAAGAACAAAGGT |
| **FOXA2** | Fwd: GGAACACCACTACGCCTTCAAC<br>Rev: AGTGCATCACCTGTTCGTAGGC<br>Probe: ACCCGTTCTCCATCAACAACCTCA |
| **NEUROD1** | Fwd: AGGACCTACTAACAACAAAGGAAA<br>Rev: TCGTCCTGAGAACTGAGACA<br>Probe: AAATCGTACAGCGAGAGTGGGCTG |
| **POU3F2** | Fwd: GGTATGGGAACTGGCCTTTAG<br>Rev: GAACTCCAGCTTCTGACCTTAC<br>Probe: TGAAGCTATCCAGAGCAGGGCAAA |
| **SOX2** | Fwd: GGAGAGTAAGAAACAGCATGGA<br>Rev: GTGGATGGGATTGGTGTTCT<br>Probe: TCCCATCACCCACAGCAAATGACA |
| **ASCL1** | Fwd: GTCGGACGAGGGCTCTTA<br>Rev: GATCACCCTGCTTCCAAAGT<br>Probe: TTGGTGAAGTCGAGAAGCTCCTGC |
| **PDX1** | Fwd: GAAGTCTACCAAAGCTCACGCG<br>Rev: GAGATGTACTTGTTGAATAGGAACTCCTTC<br>Probe: AAACATCGATCGGGCCTTGTTTGC |
| **E2F1** | Fwd: GGACTCTTCGGAGAACTTTCAG<br>Rev: TGATCCCACCTACGGTCTC<br>Probe: AAACATCGATCGGGCCTTGTTTGC |
| **ONECUT2** | Fwd: GTGGCCCAGAGGAATGAAATAG<br>Rev: GCAGAGGTAGCACTGTACAATAAG<br>Probe: AGAGTGAAAGCCCACACATGCCTC |
| **TACSTD2** | Fwd: CAGGGTCTCCTTTCTTTCTCAC<br>Rev: CTATGCCATCCCTTCCTTCAC<br>Probe: TCGGTCCAACAACAGGAAACCTGA |

## 2.5 Clinical patient samples

Fourteen samples of patients with metastatic prostate cancer were collected at different volumes, ranging from 14 – 20 mL. To be exact, the patients were adult men with metastatic castration-resistant prostate cancer who had disease progression while receiving abiraterone acetate (abiraterone) and prednisone therapy. Patients had histologically confirmed prostate adenocarcinoma without significant smallcell/ neuroendocrine or other variant histologies. In addition, participants had rising PSA values by at least one week, not showing a decline, while on abiraterone therapy.
Five healthy donor samples, of 20 mL, were obtained by blood draw from adult men.

## 2.6 Statistics and Bioinformatics

All statistical analyses were performed using the GraphPad Prism software version 9. Unless otherwise stated, data are expressed as mean values ± standard deviation (SD) of n ≥ 3 independent experiments. Two-tailed unpaired t-test (Welch's test) was used to compare differences between two or multiple groups, respectively. Differences were considered significant at $p$ <0.05.
All bioinformatical analyses were performed using the R Studio software Version 1.2.5001.

# 3 Results

## 3.1 Several cell lines carry the to-be-inspected neuroendocrine genes

ddPCR was chosen as a method to measure metastatic PC transcriptional signatures in CTC, because it has shown to be a highly sensitive application [43]. In every ddPCR experiment, a target-of-interest-carrying control template must be present to verify every analysis. To find a suitable cell line, that can serve as a positive control template the Cancer Cell Line Encyclopedia mRNA expression data (accessed March 24$^{th}$ 2022), publicly provided by Broad Institute, was used as a database. The data were filtered for all defined genes of interest in R Studio. This analysis gave a list of possible relevant cell lines. As mentioned before, PC3, VCaP, LNCaP, 22RV1, HOP62 and NCI-H727 were chosen as respective cell lines. These cell lines were chosen because of high expression (all > 1.8 RPM, RPM: reads per million mapped reads) per genes of interest and availability in the Miyamoto lab.

The next step was to evaluate the expression of the genes of interest (Table 1) in healthy donors compared to expression in PC3, VCaP, LNCaP, 22RV1, HOP62 and NCI-H727. To investigate this issue a bulk RNA-Seq data set of 19 healthy donors was provided by the Miyamoto Lab and analyzed by using R Studio. Blood samples from these 19 healthy donors were processed by using the CTC-iChip, to simulate the same process as for patient blood samples.

14 out of the 15 selected genes, show >1 RPM distinction between donor and cell line data. In *ONECUT2* we could not detect a significant difference in expression between 22RV1 and healthy donors (Figure 9). The mean of *ONECUT2* expression in healthy donors was 2.57 Reads per million reads (RPM) compared to the expression in 22RV1 cell line which was 3.20 RPM. This difference was lower than 1 RPM which led us to result that in ddPCR detection the positive control cell line (22RV1) cannot be distinguished from healthy donor samples. Taking this into consideration, ONECUT2 primers were not ordered, leaving us with 14 primer pairs (Table 7) to investigate for sensitivity and specificity.

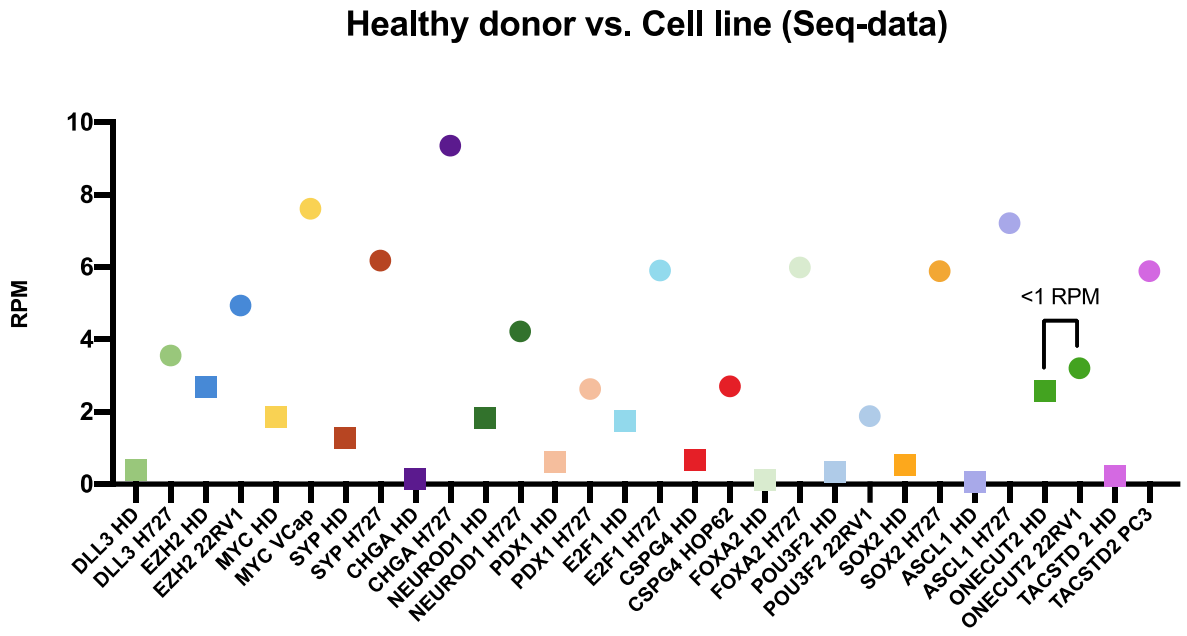


Figure 10: RNA-Seq data of gene expression in healthy donors in comparison to the cell line with the highest RPM score. The value of expression of ONECUT2 in healthy donors is in close range to the expression in 22RV1 cells. All other gene expression profiles show a distinguishing difference in healthy donors and corresponding cell line.

Abbreviations: HD healthy donor, RPM reads per million reads

## 3.2 Signal in white blood cells minimized the group of genes eligible to serve as neuroendocrine biomarker

Before applying the 14 designed assays (Table 7) to patient samples, their expression levels in white blood cells were evaluated.

After microfluidic isolation, the blood samples are depleted of most hematopoietic cells, leaving the samples with a $10^4$ to $10^5$ purification of CTCs, with around 500 WBCs remaining in 1 mL of the original blood sample [49]. Consequently, it is important to consider blood cell carryover, which can eventually contaminate the to-be-evaluated sample. Our approach was to design

assays for genes that either show no-to-minimal expression in leukocytes, or that are exceedingly upregulated in NEPC compared to leukocytes. The 14 designed ddPCR assays (Table 7) were tested for signals in white blood cells of a healthy male donor.

Seven assays exhibited high expression in white blood cells (Figure 11): POU3F2 (736 transcripts/rxn), EZH2 (590 transcripts/rxn), SOX2 (690 transcripts/rxn), ASCL1 (732 transcripts/rxn), CSPG4 (714 transcripts/rxn), TACSTD2 (660 transcripts/rxn) and FOXA2 (696 transcripts/rxn). The E2F1 assay showed a minimal expression in WBC with 3 transcripts/rxn. NEUROD1, DLL3, MYC, SYP; PDX1 and CHGA displayed no signal in WBC which is a favorable feature, when utilized as a biomarker. All assays that showed zero expression and E2F1, which showed minimal expression, were chosen to be applied to metastatic prostate cancer patient samples. In addition, we also decided to use the EZH2 assay on patient samples, because of the gene's prominent role in neuroendocrine transdifferentiation.
In total, eight assays were chosen to be applied to further analysis with cell spike-in samples and patient samples.

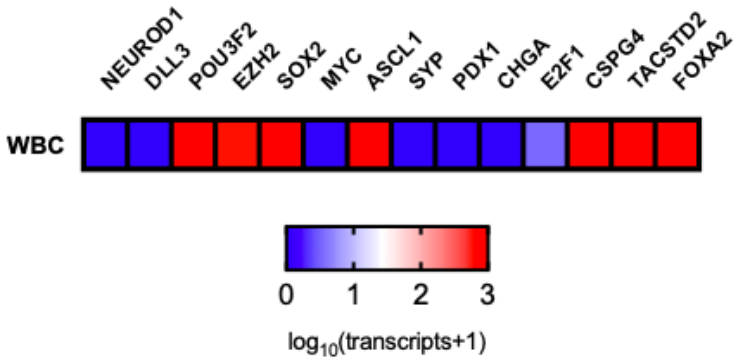


Figure 11: Heat map expression signal of each to-be-investigated gene in white blood cells (WBC), detected by ddPCR. The WBCs were obtained from a healthy male donor. High expression was detected in POU3F2, EZH2, SOX2, ASCL1, CSPG4, TACSTD2, and FOXA2 assays.

## 3.3 Digital droplet PCR analysis of spike-in samples analysis validated several designed assays

As previously mentioned, CTCs are very rare cells, and their enrichment can be a tedious process. To validate the sensitivity of our assays we spiked 1, 3, 10, and 50 cancer cell line cells into healthy male donor blood. These conditions mimic the number of CTCs which could possibly be isolated from a prostate cancer patient sample.
By analysis of the CCLE database, the lung cancer cell line H727 was found to be a carrier of all eight genes (*NEUROD1, DLL3, EZH2, MYC, SYP, PDX1, CHGA, E2F1*). Given this information, H727 cells were spiked into healthy donor blood, to resemble the cell count of CTCs in a prostate cancer patient.

To simulate clinical blood samples from cancer patients with varying degrees of tumor burden, we spiked-in 1, 3, 10, and 50 H727 cells in 4mL whole blood aliquots, before processing them through the CTC-iChip 2.0.
Following microfluidic enrichment, the samples were quantified by ddPCR. In total, five spike-in samples were processed which are displayed in Figure 12.

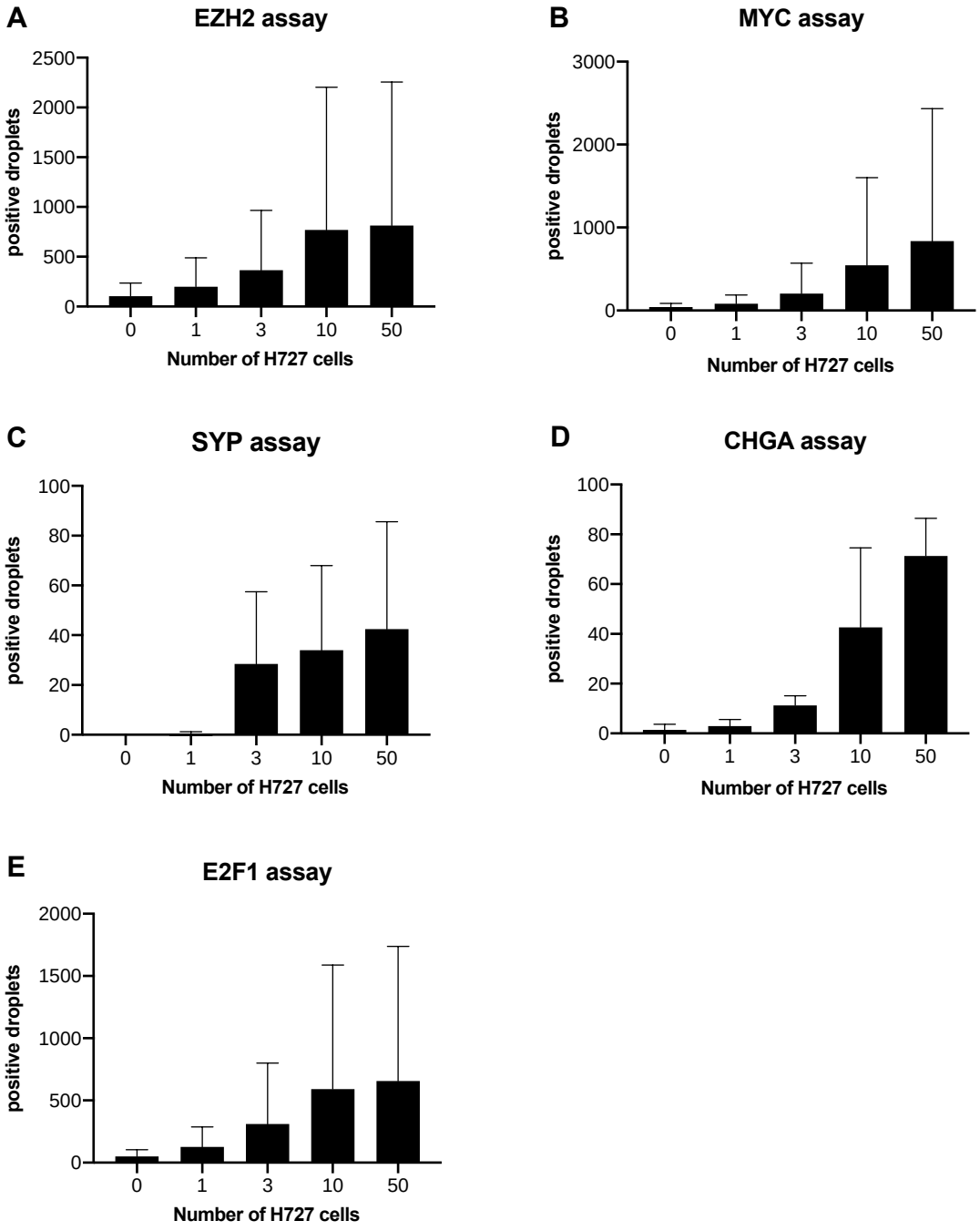


Figure 12: Bar graphs (mean value) of varying numbers of H727 cells micromanipulated into male healthy donor blood (n=5) and processed utilizing the CTC-iChip 2.0. Five different ddPCR assays (EZH2, MYC, SYP, CHGA, E2F1) gave signal for the spiked-in cell numbers. Bar graphs are pictured with standard deviation.

The introduction of a single H727 cell into healthy donor blood produced 200.4 positive droplets for the *EZH2* assay (SD = 289.3). The signal for 3, 5, 10, and 50 cells increased progressively resulting in 814.8 positive droplets (SD = 1441.4) for 50 cells. The *MYC* assay generated 38.4 positive droplets (SD = 47.1) for one spiked-in cell and 838.0 positive droplets (SD = 1595.3) for 50 spiked-in cells. Applying the *SYP* assay, 0.5 positive droplets (SD = 0.7) for one spiked-in cell and 42.5 positive droplets (SD = 43.1) for 50 spiked-in cells, were measured. The *CHGA* assay generated 3.0 positive droplets (SD = 2.6) for one spiked-in cell and 71.3 positive droplets (SD = 125.0) for 50 spiked-in cells. Finally, the *E2F1* assay produced 126.8 positive droplets (SD = 160.5) for one spiked-in cell and 656.8 positive droplets (SD = 1080.9) for 50 spiked-in cells. The increase in ddPCR signal in the prostate lineage transcripts mentioned (EZH2, MYC, SYP, CHGA, E2F1) was comparable with rising numbers of H727 cells present in the blood aliquots. High standard deviations in *EZH2*, *MYC*, *SYP* and *E2F1* spike-in samples may stem from an insufficient cDNA amplification step.

Assays for *DLL3, NEUROD1*, and *PDX1* did not generate positive droplets with the previously mentioned cell spike-in conditions. The results could stem from a low gene expression profile in H727 cells. CCLE data showed an expression of 3.55 RPM for *DLL3*, 4.22 RPM for *NEUROD1*, and 2.63 RPM for *PDX1*. The other five genes (*EZH2, MYC, SYP, CHGA, E2F1*) display expression > 4.9 RPM, which can be defined as a cut-off value, in the H727 cell line. Another reason for obtaining no signal could be that the spiked-in cells were not transferred in the CTC-iChip and remained attached to the preparation tube, in which the samples were incubated with beads and antibodies.

To generate a comparable distribution of the three assays *DLL3*, *NEUROD1*, and *PDX1*, another approach was devised. We generated a dilution series of the previously synthesized cDNA, which was directly derived from H727 cell line mRNA, and applied it as sample input in ddPCR. In this experiment diluted H727 cDNA templates were measured in ddPCR without being introduced to whole blood and without being processed with the CTC-iChip.

## 3.4 Cell line cDNA digital droplet PCR analysis gave information on assay sensitivity

The low-abundance targets *DLL3*, *NEUROD1*, and *PDX1* showed no result for the spike-in samples. Consequently, some further verification of these assays needed to be done. Therefore, we attempted to show a dilution series imitating the same conditions (0, 1, 3, 10, 50 cells) as the spike-in samples. It is a known fact, that mammalian cells contain around 10 pg total RNA/cell [60].

The 1 ng/µl concentrated H727 cDNA was used as the initial starting concentration. It was diluted in decreasing steps to a minimum concentration of 15.625 pg/µL imitating a 1.5625-cell equivalent. The H727 cDNA sample concentrations that were used in ddPCR analysis are listed in table 8.

Table 8: Seven dilution points of H727 cDNA used as template for ddPCR assay. The cDNA starting concentration of 1000pg/µl was diluted 1:2 six times to obtain all concentration points.

| Concentration [ pg / µL ] | Cell equivalent |
|---|---|
| 1000 | 100 |
| 500 | 50 |
| 250 | 25 |
| 125 | 12.5 |
| 62.5 | 6.25 |
| 31.25 | 3.125 |
| 15.625 | 1.5625 |

Figure 13 shows the individual expression profiles of the eight chosen assays for several H727 concentrations, evaluated by ddPCR signal. Seven dilution points were measured. CHGA showed the highest, and PDX1 exhibited the lowest expression in H727 cells.
With this experiment, we could provide a reference of low expression of *NEUROD1*, *DLL3*, and *PDX1* in the cancer cell line H727.
To conclude, the H727 cell line shows different expression levels of the eight evaluated assays. With this information collected, we proceeded to apply our designed assay to metastatic PC samples.

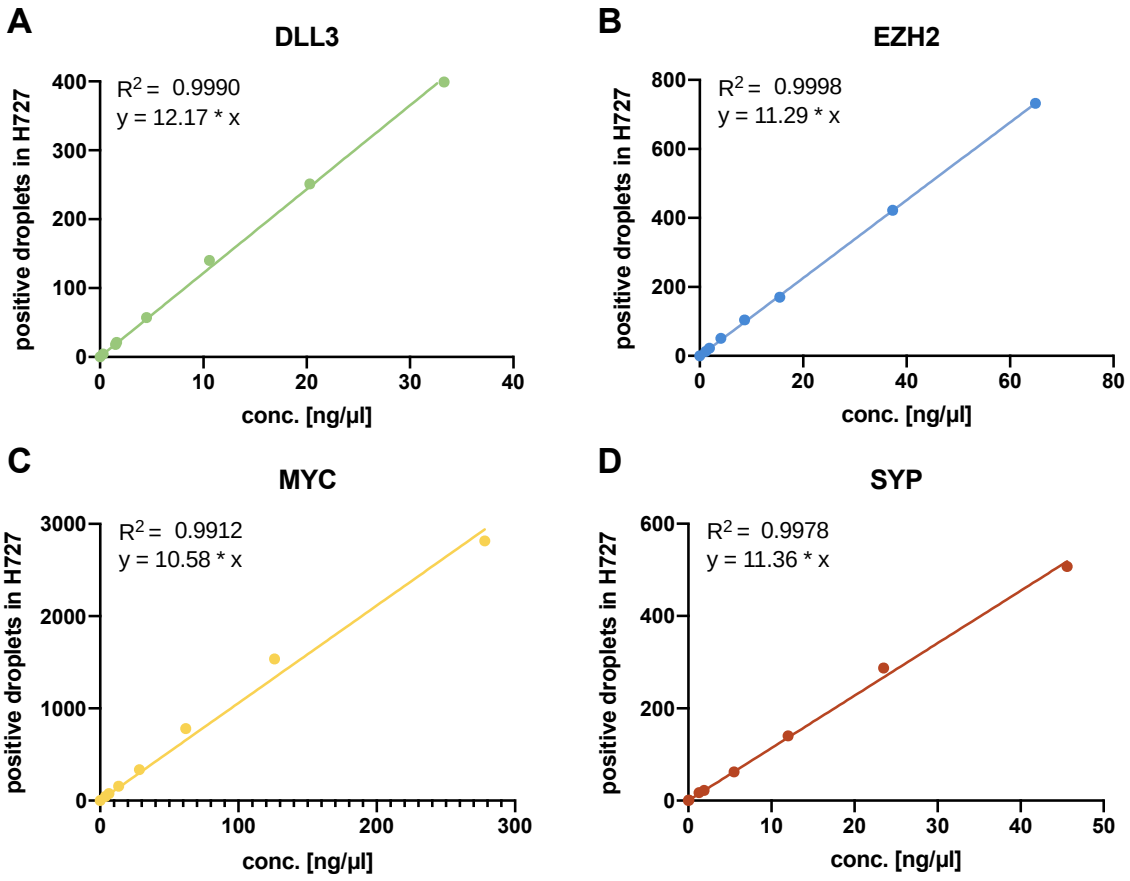

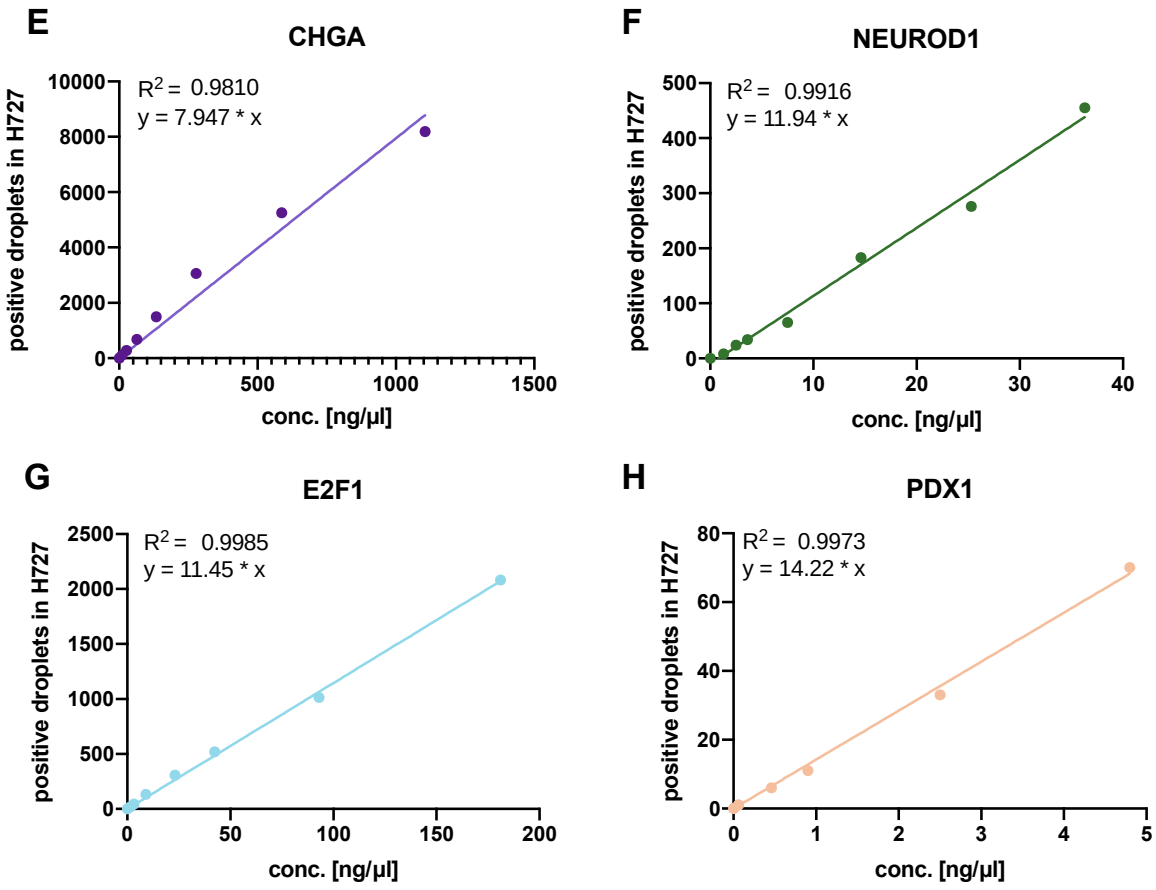


Figure 13: Scatter plots of seven H727 dilution points in eight different ddPCR assays of prostate lineage transcripts, depicted with corresponding linear regression curves. $R^2$ shows coefficient of determination. H727 RNA was directly isolated from cell culture and used a template input in ddPCR.

## 3.5 Detection of neuroendocrine prostate cancer-specific transcripts in CTCs

RNA-based digital PCR quantitation of CTC signatures has been shown to be a sensitive and specific method in prostate cancer patient care [43]. Our goal was to identify, if rare neuroendocrine PC-specific transcripts are expressed in CTCs isolated from whole blood of metastatic PC patients. The cohort of patients with metastatic prostate cancer had progressed on treatment with first- and second-line AR-targeting therapies. Based on the literature, we expect around 10-17% to have developed some form of NE transdifferention characteristics [15], [61]. With several previous experiments, we distinguished the applicability of our designed assays.

Whole blood samples of metastatic cancer patients were microfluidically processed with the CTC-iChip within 4 hours of being collected from patients.

Afterward, the samples were subjected to RNA extraction using the Qiagen RNeasy Micro Kit. The purified RNA was transcribed to cDNA and amplified by using SMART-Seq HT Kit (Takara). Thereafter, the double-stranded cDNA templates were analyzed by ddPCR.

With this experiment, we investigated if prostate-derived CTCs may express tissue-specific transcripts and if they could be measured with our eight designed assays. We tested 14 patients with metastatic prostate cancer, compared with 5 male healthy donors. The observed signal across all eight assays is shown in Figure 14. Among healthy individuals, very low signals were present in *DLL3, SYP, CHGA, PDX1* and *NEUROD1* assays. In contrast, expression of *EZH2*, *MYC*, and *E2F1* was detected in healthy donors. This outcome was expected, since the named genes are not exclusively cancer-specific. In metastatic prostate cancer patients, we found expression of *DLL3, EZH2, MYC* and *CHGA* in 1 out of 14 patients (7%). The patient group also showed positive signal of 3 out of 14 men (21%) in *SYP*, and *E2F1* assays. None of the patient samples were positive for *PDX1*, or *NEUROD1* expression. Expression profiles of healthy donors and mPC patients are collected in a heat map in Figure 15.

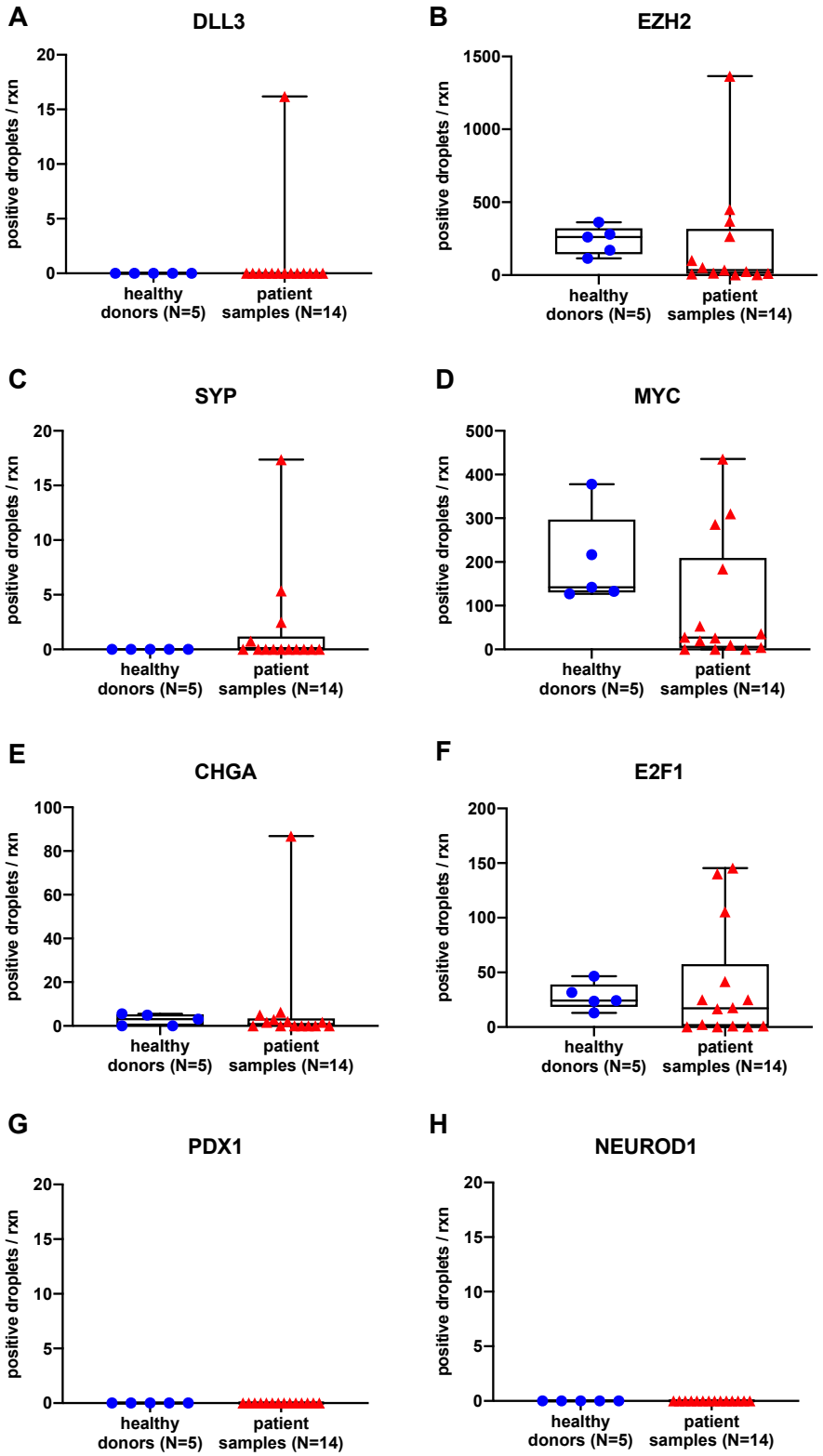


Figure 14: Graphs showing ddPCR signal for different NE gene in 14 metastatic prostate cancer patients compared to 5 healthy male control subjects. Statistical testing was done with unpaired t test (Welch's test). (A) P value: 0.3356, (B) P value: 0.7959, (C) P value: 0.1649, (D) P value: 0.1343, (E) P value: 0.4487, (F) P value: 0.5482.

For *EZH2*, *MYC*, and *E2F1* assays the measured mean expression in healthy donors was elevated compared to cancer patients. Taking this into consideration, the applicability of these assays as a biomarker tool needs to be further discussed.
In total, we found upregulation in specific NE genes in 6 (P-01-069, P-01-071, P-01-073, P-03-074, P-02-076, P-02-081) out of the 14 patients (42%).

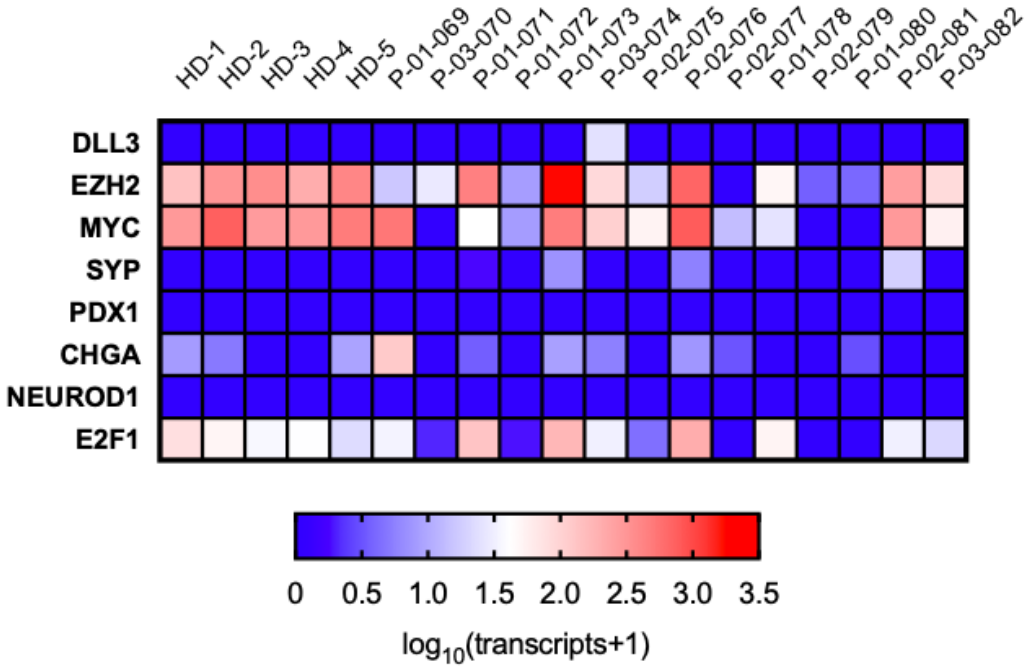


Figure 15: Heatmap compilation of eight different NE-specific assays tested by ddPCR on 14 metastatic cancer patients and 5 healthy male donors.

# 4 Discussion

## 4.1 Several newly designed neuroendocrine prostate cancer-specific assays match results from established prostate cancer assays

In 2018, Miyamoto *et al.* published the application of nine highly specific and sensitive ddPCR assays for utilization as noninvasive liquid biopsies of prostate cancer [43].
The genes targeted in the Miyamoto Lab assays include androgen-responsive transcripts *KLK2*, *KLK3*, *TMPRSS2*, *AGR2*, and androgen-repressed transcripts *HOXB13*, *FOLH1,* and androgen-independent transcripts *FAT1* and *STEAP2*. Additionally, Miyamoto *et al.* have designed a test measuring *AR-V7* signal, which has been shown to be a biomarker for gained independence in the androgen pathway, predicting resistance to enzalutamide or abiraterone

therapy. Thereof, investigating new targets in CRPC, eventually developing into NEPC, is highly relevant for clinical patient care.

The heatmap, Figure 16, is an overview of the newly designed assay, discussed in this thesis, and the nine established assays (Miyamoto *et al.,* 2018) applied to metastatic prostate cancer samples from our study.
Notably, Miyamoto *et al.* identified that patients with elevated *HOXB13* expression, are prone to be in a state of progressed disease. Several patients with positive HOXB13 signals additionally showed a heightened expression for one or more new assays detecting NE gene markers.
Patient 01-69, showed positive signal in *HOXB13, MYC, CHGA,* and *KLK3*. Patient 01-73 displayed especially high *EZH2* expression in addition to *MYC, SYP, E2F1,* and *HOXB13* positive signal. *EZH2, MYC, E2F1*, and *HOXB13* exhibited heightened expression, in patient 02-76.

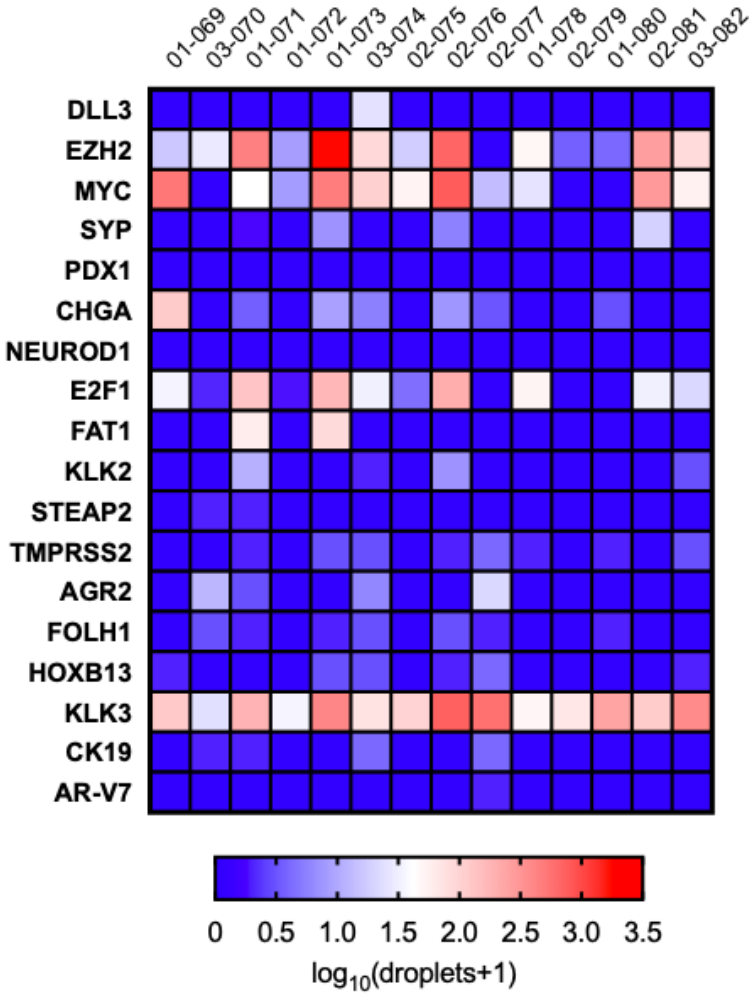


Figure 16: Heatmap of ddPCR CTC signal after whole transcriptome amplification for blood samples from metastatic prostate cancer patients. This graphic includes the depiction of assays introduced by Miyamoto *et al.,* and assays designed for this thesis [43].

To conclude, elevated expression in *HOXB13* assay, and several newly designed neuroendocrine prostate cancer-specific assays was found in several patient samples. These results could be an indication of disease progression in said prostate cancer patients. The outcomes will be further analyzed in the discussion section.

## 4.2 DLL3, SYP, CHGA RNA-based digital droplet PCR presented results in accordance with established prostate biomarker tests

The transdifferentiation from adenocarcinoma to the neuroendocrine phenotype is a highly relevant topic in prostate cancer care. Despite various improvements in the treatment of small-cell NEPC in the last decade, the overall survival rate is extremely poor with less than one-year median time [61]. The aim of this thesis was to detect hallmark genes, of the NE prostate cancer phenotype, and their expression profiles by using sensitive molecular biology methods. In recent years, liquid biopsy has emerged as a practical tool to portray tumor progression over time. These blood-based tests can detect RNA signatures from circulating tumor cells [43]. A significant advantage of CTC analysis is that real-time information on cancer cell evolution and the mechanism of resistance to therapy is obtained. Another benefit of CTC analysis is, that tumor RNA expression levels, which are necessary for examining the cell states such as NE differentiation, can be detected. In contrast, circulating tumor DNA (ctDNA) investigation can only give information on DNA mutations and aberrations [62].
In this project, we investigated some novel biomarkers (Table 7) in the detection of NEPC from CTC-derived transcripts. We reported six genes (*DLL3, EZH2, MYC, SYP, CHGA, E2F1*) that showed elevated expression in metastatic prostate cancer patients compared to a healthy donor control group. In our study, CTCs were enriched microfluidically with the CTC-iChip 2.0, which has been shown to be a reliable high-throughput isolation method [47]. After obtaining viable CTCs, we used highly sensitive ddPCR to detect mRNA transcripts.

Previous studies have already confirmed the role of *DLL3, EZH2, MYC, SYP, CHGA, E2F1* genes in prostate cancer progression [14].
The analyses of 14 patient samples confirmed our assumption that some metastatic patients might show expression of NE target genes. This hypothesis was based on previous findings, diagnosing around 10-17% of patients with metastatic disease with the NE phenotype [15], [61].
Puca *et al.* found that *DLL3* is expressed in a subset of advanced metastatic prostate cancer patients. The group found *DLL3*-positive samples in 76.6% of castration-resistant neuroendocrine prostate tumors and in 12.5% of castration-resistant adenocarcinomas. DLL3 expression was detected in 7% of the patient group, which can lead us to believe that only a few study participants suffer from further advanced disease.

Since the aim was to investigate markers for progressed prostate cancer transdifferentiating into the small-cell NE phenotype, samples with *HOXB13* expression could give information on NE biomarkers. Expression of *HOXB13* in CTCs is of particular interest since it is a lineage-specific regulator of AR transcriptional activity. Furthermore, altered AR-signaling contributes to the lowering of effectiveness of AR-targeted therapies, such as abiraterone. Miyamoto *et al.* correlated *HOXB13* overexpression with lymph node invasion and therefore consequently early death (< 1 year) [43].
Expression of *SYP* and *CHGA* has been defined as a critical point of transdifferentiated NE final state [24], [15], [24], [63]. We found elevated *SYP* expression in 3 patients, of whom 2 (patients 01-73 and 02-76) also showed enhanced *HOXB13* expression levels. The same outcome was observed in our designed *CHGA* assay. Patient 01-69 exhibited positive ddPCR signal for *CHGA* and *HOXB13* (Figure 16).
The genomic loss of *RB1* has been connected to the upregulation of *E2F1* [64]. Three metastatic cancer patients have shown high expression of *E2F1* (patients 01-71, 01-73 and 02-76). Nevertheless, *E2F1*, like *MYC* and *EZH2*, are genes not exclusively linked to cancer. It has to be acknowledged that mean values of the *MYC* and *EZH2* assays in prostate cancer patients were lower than in the healthy donor control group (Figure 14). The *MYC* assay measured a mean of 199.3 for healthy males, compared to 99.46 for metastatic prostate cancer patients. For *EZH2,* HD mean was 237.9, in contrast to 207.9, which was measured as the mean in the PC patient group. These indications draw the conclusion that the current design of the *MYC* and *EZH2* assays is not suited to be applied as a reliable NE biomarker.
No positive ddPCR signals were found in the *NEUROD1* and *PDX1* assay, therefore, their relevance as utilization as biomarker needs to be reviewed.
In total, we could demonstrate a successful application of our workflow. The experiment arrangement has several advantages. Untagged, viable CTC populations were captured with the use of the CTC-iChip 2.0. Conceptually, the application of *DLL3*, *SYP*, and *CHGA* digital RNA-based PCR assays was successfully evaluated in metastatic prostate cancer patients. The results of the named assays were in accordance with established biomarker tests by Miyamoto *et al.*.
In the future, these findings can be implemented in a broader study. The continued investigation of known neuroendocrine hallmark genes, in samples that have been histologically validated as neuroendocrine phenotype, is recommended. Additional to RNA analysis, other orthogonal approaches could be used to confirm the NE phenotype of CTCs. These concepts could include immunofluorescence-based protein assays, as well as DNA sequencing to evaluate for hallmark aberrations such as *TP53* and *Rb1* loss.

## 4.3 Future directions and project conclusion

Considering the fact that CTCs are very rare and heterogenous cells, enrichment technologies need to prioritize the approach to process a large volume of blood, which will result in obtaining a high yield of CTCs. Collecting numerous numbers of blood tubes from a cancer patient is currently prohibited. To circumvent this issue, CTCs could be isolated from a leukapheresis

product. Leukapheresis is a well-tolerated routine clinical procedure where mononucleated cells in peripheral blood are enriched by centrifugal processing [47], [65]. Though, large volumes are incompatible with current microfluidic CTC isolation applications. Mishra *et al.* recently addressed these shortcomings, by introducing a microfluidic device, the $^{LP}$CTC-iChip, for a high-throughput isolation of CTCs from an entire leukapheresis product. This new technology enables the collection of > 1000 CTCs through interrogation of > 2L blood, thus providing sufficient numbers of CTCs to serve as a potential alternative to biopsies for real-time molecular profiling and monitoring of lineage plasticity [65].

In conclusion, the so-called liquid biopsy concept can introduce novel blood-based tests, which provide a non-invasive real-time picture of a patient's malignant disease.
These contributions will be significant because they are expected to act as an addition to tissue biopsy for monitoring treatment-induced lineage plasticity, as well as provide a strong scientific framework for the design of future possible clinical trials to treat lethal NE phenotype prostate cancers. By investigating NE transdifferentiation as a key measurement, we are addressing a poorly understood but high-impact clinical phenomenon that may occur more frequently as earlier use of AR- targeted therapies becomes increasingly common in prostate cancer treatment.

# Bibliography


[1] R. L. Siegel, K. D. Miller, H. E. Fuchs, and A. Jemal, “Cancer Statistics, 2021,” *CA. Cancer J. Clin.*, vol. 71, no. 1, pp. 7–33, 2021, doi: 10.3322/caac.21654.

[2] H. E. Taitt, “Global Trends and Prostate Cancer: A Review of Incidence, Detection, and Mortality as Influenced by Race, Ethnicity, and Geographic Location,” *Am. J. Mens. Health*, vol. 12, no. 6, p. 1807, Nov. 2018, doi: 10.1177/1557988318798279.

[3] R. J. Rebello *et al.*, “Prostate cancer,” *Nat. Rev. Dis. Prim.*, vol. 7, no. 1, 2021, doi: 10.1038/s41572-020-00243-0.

[4] L. T. Aaron, O. E. Franco, and S. W. Hayward, “Review of Prostate Anatomy and Embryology and the Etiology of BPH,” *Urol. Clin. North Am.*, vol. 43, no. 3, p. 279, Aug. 2016, doi: 10.1016/J.UCL.2016.04.012.

[5] K. Fujita and N. Nonomura, “Role of Androgen Receptor in Prostate Cancer: A Review,” *World J. Mens. Health*, vol. 37, no. 3, p. 288, Sep. 2019, doi: 10.5534/WJMH.180040.

[6] D. Ilic, M. M. Neuberger, M. Djulbegovic, and P. Dahm, “Screening for prostate cancer,” *Cochrane database Syst. Rev.*, vol. 2013, no. 1, Jan. 2013, doi: 10.1002/14651858.CD004720.PUB3.

[7] G. P. Swanson, S. Trevathan, K. A. P. Hammonds, V. O. Speights, and M. R. Hermans, “Gleason Score Evolution and the Effect on Prostate Cancer Outcomes,” *Am. J. Clin. Pathol.*, vol. 155, no. 5, pp. 711–717, May 2021, doi: 10.1093/AJCP/AQAA130.

[8] P. Rawla, “Epidemiology of Prostate Cancer,” *World J. Oncol.*, vol. 10, no. 2, p. 63, 2019, doi: 10.14740/WJON1191.

[9] M. K. H. Hong *et al.*, “Tracking the origins and drivers of subclonal metastatic expansion in prostate cancer,” *Nat. Commun. 2015 61*, vol. 6, no. 1, pp. 1–12, Apr. 2015, doi: 10.1038/ncomms7605.

[10] S. Sumanasuriya and J. De Bono, “Treatment of Advanced Prostate Cancer—A Review of Current Therapies and Future Promise,” *Cold Spring Harb. Perspect. Med.*, vol. 8, no. 6, Jun. 2018, doi: 10.1101/CSHPERSPECT.A030635.

[11] M. Ahmed and R. Eeles, “Germline genetic profiling in prostate cancer: Latest developments and potential clinical applications,” *Futur. Sci. OA*, vol. 2, no. 1, Mar. 2016, doi: 10.4155/FSO.15.87/SUPPL_FILE/FSO-02-87-S1.DOCX.

[12] C. Magi-Galluzzi *et al.*, “TMPRSS2-ERG gene fusion prevalence and class are significantly different in prostate cancer of Caucasian, African-American and Japanese patients,” *Prostate*, vol. 71, no. 5, pp. 489–497, Apr. 2011, doi: 10.1002/PROS.21265.

[13] K. Desai, J. M. McManus, and N. Sharifi, “Hormonal Therapy for Prostate Cancer,” *Endocr. Rev.*, vol. 42, no. 3, pp. 354–373, Jun. 2021, doi: 10.1210/ENDREV/BNAB002.

[14] Y. Wang *et al.*, “Molecular events in neuroendocrine prostate cancer development,” *Nature Reviews Urology*, vol. 18, no. 10. Nature Publishing Group, pp. 581–596, Jul. 21, 2021, doi: 10.1038/s41585-021-00490-0.

[15] G. K. Patel, N. Chugh, and M. Tripathi, “Neuroendocrine Differentiation of Prostate Cancer—An Intriguing Example of Tumor Evolution at Play,” *Cancers (Basel).*, vol. 11,

no. 10, 2019, doi: 10.3390/CANCERS11101405.

[16] H. Beltran *et al.*, “The role of lineage plasticity in prostate cancer therapy resistance,” *Clin. Cancer Res.*, vol. 25, no. 23, pp. 6916–6924, 2019, doi: 10.1158/1078-0432.CCR-19-1423.

[17] S. Zelivianski, M. Verni, C. Moore, D. Kondrikov, R. Taylor, and M. F. Lin, “Multipathways for transdifferentiation of human prostate cancer cells into neuroendocrine-like phenotype,” *Biochim. Biophys. Acta*, vol. 1539, no. 1–2, pp. 28–43, May 2001, doi: 10.1016/S0167-4889(01)00087-8.

[18] W. Butler and J. Huang, “Neuroendocrine cells of the prostate: Histology, biological functions, and molecular mechanisms,” *Precis. Clin. Med.*, vol. 4, no. 1, pp. 25–34, Mar. 2021, doi: 10.1093/PCMEDI/PBAB003.

[19] E. M. Garabedian, P. A. Humphrey, and J. I. Gordon, “A transgenic mouse model of metastatic prostate cancer originating from neuroendocrine cells,” *Proc. Natl. Acad. Sci. U. S. A.*, vol. 95, no. 26, pp. 15382–15387, Dec. 1998, doi: 10.1073/PNAS.95.26.15382.

[20] W. Abida *et al.*, “Genomic correlates of clinical outcome in advanced prostate cancer,” *Proc. Natl. Acad. Sci. U. S. A.*, vol. 166, no. 23, pp. 11428–11436, 2019, doi: 10.1073/PNAS.1902651116/-/DCSUPPLEMENTAL.

[21] R. Aggarwal *et al.*, “JOURNAL OF CLINICAL ONCOLOGY Clinical and Genomic Characterization of Treatment-Emergent Small-Cell Neuroendocrine Prostate Cancer: A Multi-institutional Prospective Study,” *J Clin Oncol*, vol. 36, pp. 2492–2503, 2018, doi: 10.1200/JCO.

[22] “Androgen-independent prostate cancer progression in the TRAMP model - PubMed.” https://pubmed.ncbi.nlm.nih.gov/9354422/ (accessed Oct. 19, 2022).

[23] D. Lin *et al.*, “High fidelity patient-derived xenografts for accelerating prostate cancer discovery and drug development,” *Cancer Res.*, vol. 74, no. 4, pp. 1272–1283, Feb. 2014, doi: 10.1158/0008-5472.CAN-13-2921-T.

[24] H. Beltran *et al.*, “Molecular characterization of neuroendocrine prostate cancer and identification of new drug targets,” *Cancer Discov.*, vol. 1, no. 6, pp. 487–495, Nov. 2011, doi: 10.1158/2159-8290.CD-11-0130.

[25] S. Y. Ku *et al.*, “Rb1 and Trp53 cooperate to suppress prostate cancer lineage plasticity, metastasis, and antiandrogen resistance,” *Science*, vol. 355, no. 6320, Jan. 2017, doi: 10.1126/SCIENCE.AAH4199.

[26] A. M. Aparicio *et al.*, “Combined Tumor Suppressor Defects Characterize Clinically Defined Aggressive Variant Prostate Cancers,” *Clin. Cancer Res.*, vol. 22, no. 6, pp. 1520–1530, Mar. 2016, doi: 10.1158/1078-0432.CCR-15-1259.

[27] Z. Zhou *et al.*, “Synergy of p53 and Rb deficiency in a conditional mouse model for metastatic prostate cancer,” *Cancer Res.*, vol. 66, no. 16, pp. 7889–7898, Aug. 2006, doi: 10.1158/0008-5472.CAN-06-0486.

[28] E. Dardenne *et al.*, “N-Myc Induces an EZH2-Mediated Transcriptional Program Driving Neuroendocrine Prostate Cancer,” *Cancer Cell*, vol. 30, no. 4, pp. 563–577, Oct. 2016, doi: 10.1016/J.CCELL.2016.09.005.

[29] P. Mu *et al.*, “SOX2 promotes lineage plasticity and antiandrogen resistance in TP53- and RB1-deficient prostate cancer,” *Science*, vol. 355, no. 6320, Jan. 2017, doi:

10.1126/SCIENCE.AAH4307.

[30] B. Kleb *et al.*, “Differentially methylated genes and androgen receptor re-expression in small cell prostate carcinomas,” *Epigenetics*, vol. 11, no. 3, pp. 184–193, Mar. 2016, doi: 10.1080/15592294.2016.1146851.

[31] M. A. Rubin, R. G. Bristow, P. D. Thienger, C. Dive, and M. Imielinski, “Impact of Lineage Plasticity to and from a Neuroendocrine Phenotype on Progression and Response in Prostate and Lung Cancers,” *Mol. Cell*, vol. 80, no. 4, pp. 562–577, 2020, doi: 10.1016/j.molcel.2020.10.033.

[32] L. Puca *et al.*, “Delta-like protein 3 expression and therapeutic targeting in neuroendocrine prostate cancer,” *Sci. Transl. Med.*, vol. 11, no. 484, 2019, doi: 10.1126/scitranslmed.aav0891.

[33] N. Sethi and Y. Kang, “Unravelling the complexity of metastasis - molecular understanding and targeted therapies,” *Nat. Rev. Cancer*, vol. 11, no. 10, pp. 735–748, Oct. 2011, doi: 10.1038/NRC3125.

[34] T. R. Ashworth, “A Case of Cancer in Which Cells Similar to Those in the Tumours Were Seen in the Blood after Death,” *Med. J. Aust.*, vol. 14, pp. 146–147, 1869.

[35] K. Pantel and M. R. Speicher, “The biology of circulating tumor cells,” *Oncogene*, vol. 35, no. 10, pp. 1216–1224, Mar. 2016, doi: 10.1038/ONC.2015.192.

[36] J. Massagué and A. C. Obenauf, “Metastatic colonization by circulating tumour cells,” *Nat. 2016 5297586*, vol. 529, no. 7586, pp. 298–306, Jan. 2016, doi: 10.1038/nature17038.

[37] J. P. Thiery, H. Acloque, R. Y. J. Huang, and M. A. Nieto, “Epithelial-mesenchymal transitions in development and disease,” *Cell*, vol. 139, no. 5, pp. 871–890, Nov. 2009, doi: 10.1016/J.CELL.2009.11.007.

[38] Y. Horimoto *et al.*, “Analysis of circulating tumour cell and the epithelial mesenchymal transition (EMT) status during eribulin-based treatment in 22 patients with metastatic breast cancer: A pilot study 11 Medical and Health Sciences 1112 Oncology and Carcinogenesis,” *J. Transl. Med.*, vol. 16, no. 1, pp. 1–8, Oct. 2018, doi: 10.1186/S12967-018-1663-8/TABLES/2.

[39] X. Guan *et al.*, “The prognostic and therapeutic implications of circulating tumor cell phenotype detection based on epithelial-mesenchymal transition markers in the first-line chemotherapy of HER2-negative metastatic breast cancer,” *Cancer Commun. (London, England)*, vol. 39, no. 1, Jan. 2019, doi: 10.1186/S40880-018-0346-4.

[40] F. C. Bidard *et al.*, “Circulating Tumor Cells in Breast Cancer Patients Treated by Neoadjuvant Chemotherapy: A Meta-analysis,” *J. Natl. Cancer Inst.*, vol. 110, no. 6, pp. 560–567, Jun. 2018, doi: 10.1093/JNCI/DJY018.

[41] D. Lin *et al.*, “Circulating tumor cells: biology and clinical significance,” *Signal Transduct. Target. Ther. 2021 61*, vol. 6, no. 1, pp. 1–24, Nov. 2021, doi: 10.1038/s41392-021-00817-8.

[42] T. T. Moritz Maas, Miriam Hegemann, Steffen Rausch, Jens Bedke, Arnulf Stenzl, “Circulating tumor cells and their role in prostate cancer.”

[43] D. T. Miyamoto *et al.*, “An RNA-based digital circulating tumor cell signature is predictive of drug response and early dissemination in prostate cancer,” *Cancer Discov.*, vol. 8,

no. 3, pp. 288–303, 2018, doi: 10.1158/2159-8290.CD-16-1406.

[44] D. A. Haber and V. E. Velculescu, “Blood-based analyses of cancer: Circulating tumor cells and circulating tumor DNA,” *Cancer Discov.*, vol. 4, no. 6, pp. 650–661, 2014, doi: 10.1158/2159-8290.CD-13-1014.

[45] A. J. Rushton, G. Nteliopoulos, J. A. Shaw, and R. C. Coombes, “A Review of Circulating Tumour Cell Enrichment Technologies,” *Cancers 2021, Vol. 13, Page 970*, vol. 13, no. 5, p. 970, Feb. 2021, doi: 10.3390/CANCERS13050970.

[46] M. Cristofanilli *et al.*, “Circulating Tumor Cells, Disease Progression, and Survival in Metastatic Breast Cancer,” *https://doi.org/10.1056/NEJMoa040766*, vol. 351, no. 8, pp. 781–791, Aug. 2004, doi: 10.1056/NEJMOA040766.

[47] J. F. Edd *et al.*, “Isolation of circulating tumor cells,” *iScience*, vol. 25, no. 8. Elsevier Inc., Aug. 19, 2022, doi: 10.1016/j.isci.2022.104696.

[48] Di. Han, K. Chen, J. Che, J. Hang, and H. Li, “Detection of Epithelial-Mesenchymal Transition Status of Circulating Tumor Cells in Patients with Esophageal Squamous Carcinoma,” *Biomed Res. Int.*, vol. 2018, 2018, doi: 10.1155/2018/7610154.

[49] E. Ozkumur *et al.*, “Inertial focusing for tumor antigen-dependent and -independent sorting of rare circulating tumor cells,” *Sci. Transl. Med.*, vol. 5, no. 179, 2013, doi: 10.1126/scitranslmed.3005616.

[50] J. F. Edd *et al.*, “Microfluidic concentration and separation of circulating tumor cell clusters from large blood volumes,” *Lab Chip*, vol. 20, no. 3, pp. 558–567, 2020, doi: 10.1039/c9lc01122f.

[51] F. Fachin *et al.*, “Monolithic Chip for High-throughput Blood Cell Depletion to Sort Rare Circulating Tumor Cells,” *Sci. Reports 2017 71*, vol. 7, no. 1, pp. 1–11, Sep. 2017, doi: 10.1038/s41598-017-11119-x.

[52] F. Ionescu, J. Zhang, and L. Wang, “Clinical Applications of Liquid Biopsy in Prostate Cancer: From Screening to Predictive Biomarker,” *Cancers (Basel).*, vol. 14, no. 7, 2022, doi: 10.3390/cancers14071728.

[53] S. Olmedillas-López, R. Olivera-Salazar, M. García-Arranz, and D. García-Olmo, “Current and Emerging Applications of Droplet Digital PCR in Oncology: An Updated Review,” *Mol. Diagn. Ther.*, vol. 26, no. 1, pp. 61–87, Jan. 2022, doi: 10.1007/S40291-021-00562-2.

[54] E. Navarro, G. Serrano-Heras, M. J. Castaño, and J. Solera, “Real-time PCR detection chemistry,” *Clin. Chim. Acta.*, vol. 439, pp. 231–250, 2015, doi: 10.1016/J.CCA.2014.10.017.

[55] S. J. Oh *et al.*, “Auricular cartilage regeneration with adipose-derived stem cells in rabbits,” *Mediators Inflamm.*, vol. 2018, 2018, doi: 10.1155/2018/4267158.

[56] C. M. Hindson, “Absolute quantification by droplet digital PCR versus analog real-time PCR,” *Physiol. Behav.*, vol. 176, no. 1, pp. 139–148, 2018, doi: 10.1038/nmeth.2633.Absolute.

[57] Biorad, “Droplet Digital ™ PCR Droplet Digital ™ PCR Applications Guide,” *Biorad*, p. 145, 2018, [Online]. Available: http://www.bio-rad.com/webroot/web/pdf/lsr/literature/Bulletin_6407.pdf.

[58] P. L. Quan, M. Sauzade, and E. Brouzes, “DPCR: A technology review,” *Sensors (Switzerland)*, vol. 18, no. 4, 2018, doi: 10.3390/s18041271.

[59] S. C. Taylor, G. Laperriere, and H. Germain, “Droplet Digital PCR versus qPCR for gene expression analysis with low abundant targets: from variable nonsense to publication quality data,” *Sci. Reports 2017 71*, vol. 7, no. 1, pp. 1–8, May 2017, doi: 10.1038/s41598-017-02217-x.

[60] F. Han and S. J. Lillard, “In-situ sampling and separation of RNA from individual mammalian cells,” *Anal. Chem.*, vol. 72, no. 17, pp. 4073–4079, Sep. 2000, doi: 10.1021/AC000428G.

[61] H. T. Wang, Y. H. Yao, B. G. Li, Y. Tang, J. W. Chang, and J. Zhang, “Neuroendocrine Prostate Cancer (NEPC) progressing from conventional prostatic adenocarcinoma: factors associated with time to development of NEPC and survival from NEPC diagnosis-a systematic review and pooled analysis,” *J. Clin. Oncol.*, vol. 32, no. 30, pp. 3383–3390, Oct. 2014, doi: 10.1200/JCO.2013.54.3553.

[62] I. Heidrich, L. Ačkar, P. Mossahebi Mohammadi, and K. Pantel, “Liquid biopsies: Potential and challenges,” *Int. J. cancer*, vol. 148, no. 3, pp. 528–545, Feb. 2021, doi: 10.1002/IJC.33217.

[63] S. K. Pal *et al.*, “Synaptophysin expression on circulating tumor cells in patients with castration resistant prostate cancer undergoing treatment with abiraterone acetate or enzalutamide,” *Urol. Oncol. Semin. Orig. Investig.*, vol. 36, no. 4, pp. 162.e1-162.e6, 2018, doi: 10.1016/j.urolonc.2017.12.006.

[64] C. McNair *et al.*, “Differential impact of RB status on E2F1 reprogramming in human cancer,” *J. Clin. Invest.*, vol. 128, no. 1, pp. 341–358, Jan. 2018, doi: 10.1172/JCI93566.

[65] A. Mishra *et al.*, “Ultrahigh-throughput magnetic sorting of large blood volumes for epitope-agnostic isolation of circulating tumor cells,” *Proc. Natl. Acad. Sci. U. S. A.*, vol. 117, no. 29, pp. 16839–16847, 2020, doi: 10.1073/pnas.2006388117.

# List of Figures

# List of Tables

# List of Abbreviations

| | |
|---|---|
| AB | Antibody |
| ADT | Androgen deprivation therapy |
| AR | Androgen receptor |
| ASCL1 | Achaete-scute Family bHLH Transcription Factor 1 |
| ATCC | American Type Culture Collection |
| CCLE | Cancer Cell Line Encyclopedia |
| CHGA | Chromogranin-A |
| CK | Cytokeratin |
| COC | Cyclic olefin copolymer |
| CRPC | Castration-resistant prostate cancer |
| CSPG4 | Chondroitin Sulfate Proteoglycan 4 |
| CTC | Circulating tumor cells |
| ctDNA | Circulating tumor desoxyribonucleic acid |
| ddPCR | droplet digital Polymerase Chain Reaction |
| DLL3 | Delta-like 3 |
| DRE | Digital rectal examination |
| E2F1 | E2F Transcription Factor 1 |
| EMT | Epithelial-to-mesenchymal transition |
| EpCAM | Epithelial cell adhesion molecule |
| EZH2 | Enhancer of Zeste Homolog 2 |
| FCS | Fetal calf serum |
| FDA | Food and Drug Administration |
| FOXA2 | Forkhead-Box-Protein A2 |
| IF | Inertial focusing |
| LHRH | Luteinizing hormone-releasing hormone |
| MACS | Magnetic-activated cell sorting |
| mCRPC | Metastatic castration-resistant prostate cancer |

| | |
|---|---|
| MGH | Massachusetts General Hospital |
| MM | Master mix |
| mPC | Metastatic prostate cancer |
| MRI | Magnetic resonance imaging scan |
| MYC | Myelocytomatosis |
| NE | Neuroendocrine |
| NEUROD1 | Neurogenic Differentiation 1 |
| NISA | Non-equilibrium inertia separation array |
| ONECUT2 | One Cut Homeobox 2 |
| PBS | Phosphate-buffered saline |
| PC | Prostate Cancer |
| PDX | Patient-derived xenograft |
| PDX1 | Pancreatic and Duodenal Homeobox 1 |
| POU3F2 | POU Class 3 Homeobox 2 |
| PSA | Prostate Specific Antigen |
| Rb1 | Retinoblastoma protein 1 |
| RBC | Red blood cell |
| RPM | Reads per million mapped reads |
| RT | Reverse transcribed |
| SD | Standard deviation |
| SOX2 | Sex determining Region Y-box 2 |
| SYP | Synaphtophysin |
| TACSTD2 | Tumor Associated Calcium Signal Transducer 2 |
| TNM | Tumor node metastasis |
| TP53 | Tumor protein 53 |
| TRAMP | Transgenic adenocarcinoma of the mouse prostate |
| USA | United States of America |
| WBC | White blood cell |